

A comparative analysis of the vestibular apparatus in *Epipliopithecus vindobonensis*: Phylogenetic implications

Alessandro Urciuoli ^{a,*}, Clément Zanolli ^b, Amélie Beaudet ^{a, c,d,a}, Marta Pina ^{a,e}, Sergio Almécija ^{f,g,a}, Salvador Moyà-Solà ^{a,h,i}, David M. Alba ^{a,*}

^a *Institut Català de Paleontologia Miquel Crusafont, Universitat Autònoma de Barcelona, Edifici ICTA-ICP, c/ Columnes s/n, Campus de la UAB, 08193 Cerdanyola del Vallès, Barcelona, Spain*

^b *Univ. Bordeaux, CNRS, MCC, PACEA, UMR 5199, F-33600 Pessac, France*

^c *School of Geography, Archaeology and Environmental Studies, University of the Witwatersrand, Private Bag 3, Johannesburg, WITS 2050, South Africa*

^d *Department of Anatomy, University of Pretoria, PO Box 2034, Pretoria, 0001, South Africa*

^e *School of Earth and Environmental Sciences, Faculty of Science and Engineering, University of Manchester, 176 Oxford Road, Manchester M13 9PL, UK*

^f *Division of Anthropology, American Museum of Natural History, Central Park West at 79th Street, New York, NY 10024, USA*

^g *New York Consortium in Evolutionary Primatology, New York, NY, USA*

^h *Institució Catalana de Recerca i Estudis Avançats (ICREA), Passeig de Lluís Companys 23, 08010 Barcelona, Spain*

ⁱ *Unitat d'Antropologia (Departament de Biologia Animal, Biologia Vegetal i Ecologia), Universitat Autònoma de Barcelona, Campus de la UAB s/n, 08193 Cerdanyola del Vallès, Barcelona, Spain*

*Corresponding authors.

E-mail address: alessandro.urciuoli@icp.cat (A. Urciuoli); david.alba@icp.cat (D.M. Alba).

³ Department of Archaeology, University of Cambridge, Fitzwilliam St, Cambridge CB2 1QH, UK.

Abstract

Pliopithecoids are an extinct group of catarrhine primates from the Miocene of Eurasia. More than fifty years ago, they were linked to hylobatids due to some morphological similarities, but most subsequent studies have supported a stem catarrhine status, due to the retention of multiple plesiomorphic features (e.g., the ectotympanic morphology) relative to crown catarrhines. More recently, some morphological similarities to hominoids have been noted, raising the question of whether they could be stem members of this clade. To re-evaluate these competing hypotheses, we examine the morphology of the semicircular canals of the bony labyrinth of the middle Miocene pliopithecoid *Epipliopithecus vindobonensis*. The semicircular canals are suitable to test between these hypotheses because: (1) they have been shown to embed strong phylogenetic signal and reliably discriminate among major clades; (2) several potential hominoid synapomorphies have been identified previously in the semicircular canals; and (3) semicircular canal morphology has not been previously described for any pliopithecoid. We use a deformation-based (landmark-free) three-dimensional geometric morphometric approach to compare *Epipliopithecus* with a broad primate sample of extant and extinct anthropoids. We quantify similarities in semicircular canal morphology using multivariate analyses, reconstruct ancestral morphotypes by means of a phylomorphospace approach, and identify catarrhine and hominoid synapomorphies based on discrete characters. *Epipliopithecus* semicircular canal morphology most closely resembles that of platyrrhines and *Aegyptopithecus* due to the retention of multiple anthropoid symplesiomorphies. However, *Epipliopithecus* is most parsimoniously interpreted as a stem catarrhine more derived than *Aegyptopithecus* due to the possession of a crown catarrhine synapomorphy (i.e., the rounded anterior canal), combined with the lack of other catarrhine and any hominoid synapomorphies. Some similarities with hylobatids and atelids are interpreted as

homoplasies likely related to positional behavior. The semicircular canal morphology of *Epipliopithecus* thus supports the common view that pliopithecoids are stem catarrhines.

Keywords: Pliopithecidae; Catarrhini; Miocene; Inner ear; Phylogeny; Geometric morphometrics

1. Introduction

1.1. *The phylogenetic position of pliopithecoids*

Pliopithecoids are an extinct superfamily of catarrhine primates, recorded in Eurasia from the early to the late Miocene (Andrews et al., 1996; Begun, 2002, 2017; Harrison, 2005, 2013). Their first occurrence, in the early Miocene of China (~18–17 Ma; Harrison and Gu, 1999; Begun, 2002; Harrison, 2013), slightly predates the oldest record of large-bodied apes in Eurasia (Heizmann and Begun, 2001; Casanovas-Vilar et al., 2011). In the absence of older (earliest Miocene) catarrhines in that continent, pliopithecoids are assumed to have an African origin (Harrison, 1987, 2013; Begun, 2017). Like apes, pliopithecoid ancestors probably dispersed into Eurasia before the Langhian transgression, which was possible due to the lowered sea level and tectonic events that led to the closure of the Tethys Seaway and the establishment of an intermittent terrestrial corridor beginning at ~19 Ma (Harzhauser et al., 2007; Harrison, 2013).

Decades ago, pliopithecoids were considered to be phylogenetically related to hylobatids due to some superficial resemblances in cranial morphology as well as body size and proportions (e.g., Hürzeler, 1954; Zapfe, 1958, 1960, 1961; Simons and Fleagle, 1973). Currently, they are generally considered a clade of stem catarrhines—as supported by the retention of several cranial and postcranial features that are plesiomorphic compared to the crown members of the group (Andrews, 1975; Ciochon and Corruccini, 1977; Fleagle, 1984; Harrison, 1987, 2005, 2013; Andrews et al., 1996; Begun, 2002,

2017). The divergence of pliopithecoids before the split of crown catarrhines is further supported by most recent cladistic analyses (Zalmout et al., 2010; Stevens et al., 2013; Nengo et al., 2017; Gilbert et al., 2020), implying a long ghost lineage of ca. 12–14 Myr for pliopithecoids (Begun, 2017). The exception is the cladistic analysis by Alba et al. (2015), which recovered pliopithecoids as a clade of stem hominoids—thereby eliminating the need to hypothesize a long gap in the pliopithecoid fossil record. Most recently, Almécija et al. (2019) further documented similarities in femoral morphology between pliopithecoids (*Epipliopthecus*) and extant hominoids, thereby casting additional doubts on the status of pliopithecoids as stem catarrhines. Further uncertainty in this regard stems from the fact that no tail vertebrae are known from pliopithecoids (Begun, 2017). Based on sacral morphology, Zapfe (1958, 1961) argued that no external tail would have been present, as in hominoids; although this has subsequently been rebutted (Ankel, 1965; Russo, 2016), available evidence in this regard remains uncertain.

There are multiple genera of pliopthecids (Harrison and Gu, 1999; Moyà-Solà et al., 2001; Begun, 2002, 2017; Harrison, 2005, 2013; Alba et al., 2010; Alba and Moyà-Solà, 2012; Alba and Berning, 2013; Sankhyan et al., 2017; Harrison et al., 2020), which, following Harrison et al. (2020), we provisionally group into four different families: dionysopithecids (*Dionysopithecus* and *Platodontopithecus*), krishnapithecids (*Krishnapithecus*), pliopthecids (*Pliopthecus* and *Epipliopthecus*), and crouzeliids (*Plesioptiopthecus*, *Barberapithecus*, *Anapithecus*, *Egarapithecus*, and *Laccopithecus*). However, it is noteworthy that the treatment of these genera at the family rank, and even the placing of some genera in one or another group, differs among authors (e.g., compare Alba and Moyà-Solà, 2012 with Begun, 2017). Such disagreements largely stem from the fact that the internal phylogeny of pliopthecoids is still unclear and that their affinities with fossil catarrhines from Africa remain uncertain (e.g., Harrison, 2013).

1.2. Evidence from *Epipliopithecus*

Deciphering the phylogenetic relationships of most pliopithecoids is hampered by the fact that they are mostly known by fragmentary dentognathic remains, with the exception of *Epipliopithecus vindobonensis*, whose craniodental and postcranial morphology is well documented by several skeletons from the middle Miocene (MN6, ~14.85–13.45 Ma¹) karstic infillings of Devínska Nová Ves, Slovakia (Zapfe, 1958, 1961; Andrews et al., 1996; Begun, 2002; Harrison, 2013). *Epipliopithecus* was originally established as a subgenus of *Pliopithecus* by Zapfe and Hürzeler (1957), being subsequently considered a junior subjective synonym of the latter (e.g., Andrews et al., 1996; Harrison and Gu, 1999; Moyà-Solà et al., 2001; Harrison, 2005, 2013; Alba et al., 2010) or a distinct genus (e.g., Begun, 2002; Alba and Moyà-Solà, 2012; Arias-Martorell et al., 2015; Alba et al., 2015; this study). From a locomotor viewpoint, *E. vindobonensis* has been variously depicted as an arboreal or semiterrestrial generalized quadruped with varying degrees of climbing and suspensory abilities (see discussion in Arias-Martorell et al., 2015). From a phylogenetic perspective, its purported stem catarrhine status has been supported by features such as the short and only partially enclosed ectotympanic, the presence of entepicondylar foramen in the distal humerus, and single hinge-like carpometacarpal joint in the thumb (Zapfe, 1961; Szalay and Delson, 1979; Harrison, 1987, 2005; Andrews et al., 1996; Begun, 2002, 2017).

The external morphology of the petrosal bone of *E. vindobonensis* (Zapfe, 1961; Szalay, 1975; Fricano, 2018) has been of utmost significance in the discussion of its phylogenetic affinities, given that the presence of a tubular ectotympanic is considered synapomorphic of crown catarrhines (e.g., Szalay, 1975; Szalay and Delson, 1979;

¹ Age uncertainly based on the boundaries recognized for MN6 (van der Meulen et al., 2011).

Harrison, 1987, 2005; Andrews et al., 1996; Begun, 2002; Zalmout et al., 2010; Alba et al., 2015; Nengo et al., 2017). The possibility remains that such ossification took place to some extent independently in cercopithecoids, hominoids and/or other anthropoids such as pliopithecoids (Begun, 2002, 2017; Alba et al., 2015). However, other features of *Epipliopithecus* also appear plesiomorphic as compared to crown catarrhines and show no particular similarities with hominoids, namely: the large postglenoid process separated from the acoustic meatus, as in platyrrhines (Zapfe, 1961); the lack of ossification in the tentorium cerebelli (unlike in most platyrrhines and stem anthropoids, but similar to *Aegyptopithecus* and crown catarrhines; Kay et al., 2009a); and the deep subarcuate fossa (Zapfe, 1961), as in platyrrhines and most anthropoids except hominids (Gannon et al., 1988; Kunimatsu et al., 2019). In contrast, the inner ear morphology of *Epipliopithecus* has not been described and therefore its potential phylogenetic implications remain unexplored.

1.3. The bony labyrinth of the inner ear

Among the inner cavities of the petrosal, the bony labyrinth of the inner ear is constituted by the semicircular canals (SCs) and the vestibule (which together host the soft-tissue structures linked with the sense of balance) plus the cochlea. Semicircular canal size (e.g., Spoor et al., 2007; Silcox et al., 2009; Ryan et al., 2012; Grohé et al., 2018) and orientation (David et al., 2010; Malinzak et al., 2012; Berlin et al., 2013; Perier et al., 2016; Gonzales et al., 2019) have been frequently used for inferring agility, while the shape of the canals as a whole has tentatively been linked to positional behavior (Le Maître et al., 2017). At the same time, recent studies have demonstrated that the SCs bear strong phylogenetic signal among anthropoids (Lebrun, 2010, 2012; Urciuoli et al., 2019, 2020; del Rio et al., 2020; Morimoto et al., 2020) and other mammals (e.g., Grohé et al., 2015; Menecart et al., 2016, 2017; Costeur et al., 2018).

Although adaptively relevant characters may constitute synapomorphies of particular clades, arguably their relationship with function makes them potentially more prone to homoplasy. However, the correlation between SC morphology and positional behavior has recently been questioned by some studies (i.e., Rae et al., 2016; del Río et al., 2020; Morimoto, et al., 2020), and SC shape variation has been shown to largely follow the expectations of a Brownian motion mode of evolution in both platyrrhines (del Río et al., 2020) and catarrhines (Urciuoli et al., 2020). These results are in accordance with those obtained for the bony labyrinth as a whole, showing that its morphology reflects phylogenetic relatedness as inferred from molecular data (Lebrun et al., 2010; Ekdale, 2013; Macrini, et al., 2013; Billet et al., 2015). Cumulatively, this evidence suggests that bony labyrinth morphology is phylogenetically informative among mammals (Mennecart et al., 2017) and may thus potentially illuminate the phylogenetic relationships of extinct primates. Following Mennecart and Costeur (2016), who suggested that inner ear structures might be highly informative for large cladistics analyses, Urciuoli et al. (2020) explored catarrhine SC shape variation among catarrhines and proposed several potential synapomorphies for crown hominoids.

Here we test between two different phylogenetic hypotheses for *Epipliopithecus*, one hypothesis being that *Epipliopithecus* is a stem catarrhine, the other hypothesis that *Epipliopithecus* is a hominoid, based on the information provided by the shape of the SCs and vestibule. This morphology is described here for the first time using a three-dimensional geometric morphometric (3DGM) approach applied to a broad sample of extant and fossil anthropoids (Urciuoli et al., 2020). We refrained from analyzing the entire bony labyrinth (i.e., including also the cochlea) because its potential for phylogenetic reconstruction among primates is currently unclear. A recent analysis in platyrrhines suggested that cochlear shape departs from a Brownian motion mode of evolution (Blomberg's $K < 1$; del Río et al., 2020), thus potentially reflecting a greater influence of

function (and likely homoplasy due to similar selection pressures) than is the case for the SCs and vestibule. This is in agreement with previous studies linking several macroscopic cochlear features to hearing capabilities (e.g., Manoussaki et al., 2006; Kirk and Gosselin-Ildari, 2009; Coleman and Colbert, 2010). More detailed morphometric analyses of this structure among anthropoids is thus required to determine whether cochlear morphology can be meaningfully used to decipher the phylogenetic relationships of extinct catarrhines such as *Epipliopithecus*.

2. Materials and methods

2.1. Described material

We inspected three petrosals of *E. vindobonensis* belonging to two individuals from Devínska Nová Ves, Slovakia (Zapfe, 1960, 1961): NMB OE 303a, b (individual III), left (a) and right (b), housed in the Naturhistorisches Museum of Basel, Switzerland²; and NHMW 1970/1397/0003 (individual II), right, housed in the Naturhistorisches Museum of Wien, Austria.

2.2. Comparative sample

The comparative sample includes μ CT scans of 162 dried crania and temporal bones belonging to 31 extant anthropoid species (see Supplementary Online Material [SOM] Table S1 for the sample size of the extant species), plus five fossil anthropoids (SOM Table S2): the stem anthropoid *Parapithecus* (Bush et al., 2004), the stem catarrhine *Aegyptopithecus* (Simons et al., 2007), the stem platyrrhines *Dolichocebus* (Kay et al., 2009b) and *Homunculus* (Fulwood et al., 2016), and the hominoid *Oreopithecus* (Rook et al., 2004).

² Morimoto et al. (2020) included the bony labyrinth of NMB OE 303a in their comparative study but did not depict or specifically describe its morphology.

2.3. Sample preparation

NMB OE 303 was scanned with a Phoenix Nanotom®, GE at the Biomaterials Science Centre of the University of Basel (Switzerland) obtaining a voxel size of 25 µm. NHMW 1970/1397/0003 was scanned at the Vienna µCT-Lab using a Viscom X8060 (Viscom XT9190-THP X-ray tube) obtaining a voxel size of 22 µm. The canals and vestibule of NMB OE 303a, b were filled with air, while in NHMW 1970/1397/0003 they were partially filled with sediment. In both cases we segmented the SCs and vestibule cavities using the ‘watershed’ tool of Avizo v. 9.0.1 (FEI Visualization Sciences Group, Houston), with additional manual corrections for NHMW 1970/1397/0003. The 3D surfaces of NMB OE 303b and NHMW 1970/1397/0003 were mirrored for comparison. The 3D meshes of the two individuals are available from MorphoSource (see Table 1).

Table 1

Digital object identifiers (DOIs) of the 3D virtual models of the vestibule and semicircular canals of *Epipliothecus vindobonensis* available from MorphoSource.org (<https://www.morphosource.org>).

Catalog No.	Museum	DOI
NMBOE 303a (individual III)	NMBOE	https://doi.org/10.17602/M2/M113935
NMBOE 303b (individual III)	NMBOE	https://doi.org/10.17602/M2/M113933
NHMW 1970/1397/0003 (individual II)	NHMW	https://doi.org/10.17602/M2/M113932

Abbreviations: NMB OE = Naturhistorisches Museum Basel, Switzerland; NHMW = Naturhistorisches Museum Wien, Austria.

The µCT scans of most extant comparative species and of fossil anthropoids were accessed from MorphoSource.org digital repository (<https://www.morphosource.org>) with the exception of *Oreopithecus bambolii* petrosal, which was kindly provided by Lorenzo Rook (see SOM Table S2 for voxel sizes). Further details about the µCT scans of the extant comparative sample (voxel sizes, exact source, DOI, etc.) can be found in Urciuoli et al. (2020: Supplementary File 1). The slice stacks of these crania were processed using Avizo v. 9.0.1. and the left bony labyrinth was segmented using the semiautomatic ‘watershed’ tool of Avizo (with additional manual corrections in the case of partially filled canals found in the fossil specimens) and digitally extracted; when the left bony labyrinth was unavailable, the right one was mirrored. As in Urciuoli et al. (2020), the SCs and the vestibule were separated from the cochlea by cutting the generated 3D meshes

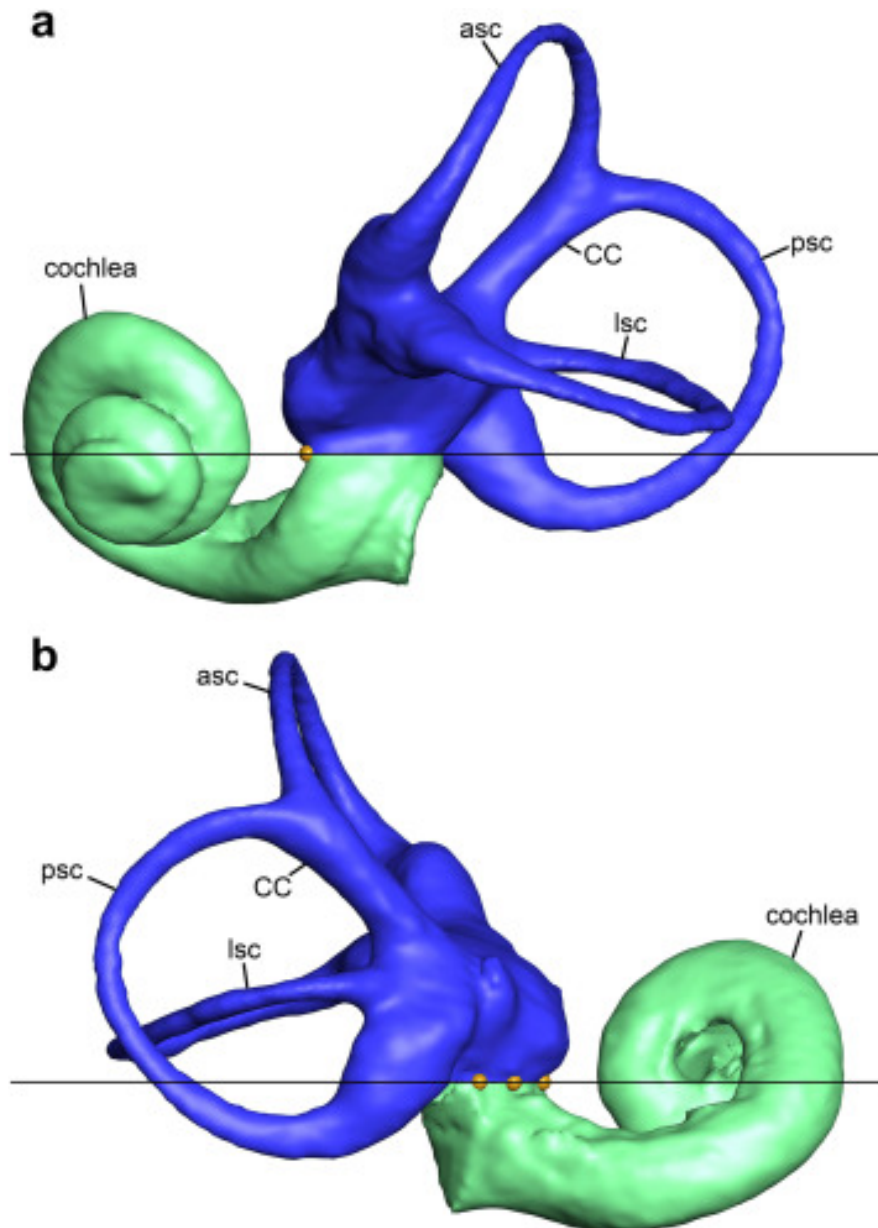


Figure 1. Illustration of the protocol used for digitally separating the cochlea (green) from the semicircular canals and the vestibule (blue). a) In anterior view, the first landmark (yellow filled circle) is placed anteriorly to the oval window, on the point of maximum surface curvature of the ridge-like morphology formed by the narrowing of the vestibule. b) In posterior view, three landmarks are placed along the junction between the bony vestibule and the cochlea, defined by the line of maximum surface curvature found immediately below the bulge formed by the saccular recess. A cutting plane (here perpendicular to the view and depicted by a black line) is best fitted to the identified landmarks using the 'Points To Fit' option of the 'Clipping Plane' module of Avizo version 9.0.1 (FEI Visualization Sciences Group, Houston) via a customized script (available upon request to A.U.), and used as a reference for a straight cut. Abbreviations: asc = anterior semicircular canal; psc = posterior semicircular canal; lsc = lateral semicircular canal; CC = common crus.

immediately inferior to the saccule and the oval window, using landmarks placed along the maximum curvature of the junction between the vestibule and the cochlea as reference for the cutting plane (Fig. 1). The resulting holes were filled with a flat surface using Geomagic Studio v. 2014.3.0 (3D Systems, Rock Hill, USA). Prior to the 3DGM analysis, the surfaces were first roughly prealigned by manually superimposing the meshes to ensure biological correspondence. Subsequently, the alignment was automatically refined using the Avizo module 'Align Surface' with the 'rigid + uniform' option. Similar to Procrustes superimposition, this module minimizes the distances between the faces of each surface by scaling, translating and rotating the analyzed meshes. The phylogenetic relationships of the extinct taxa included in the analyses, relative to extant anthropoids, are summarized in Figure 2.

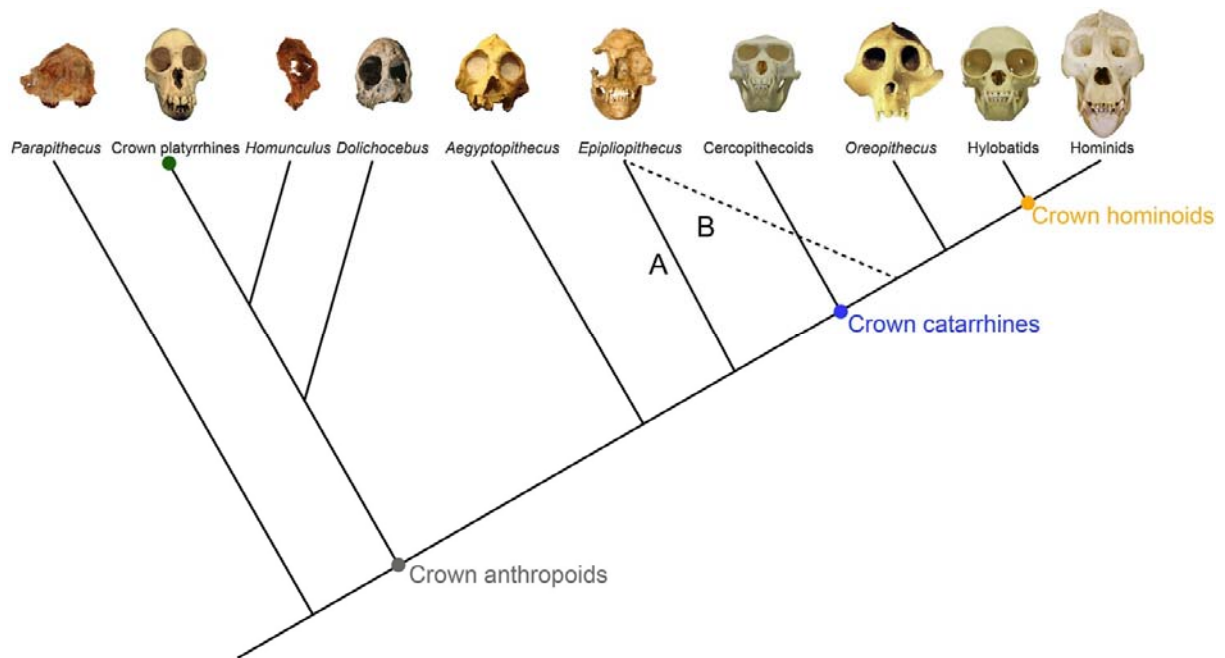


Figure 2. Cladogram of extant and fossil anthropoids showing the two phylogenetic hypotheses for *Epiplioptithecus*. The solid line (A) denotes the most widely accepted phylogenetic position of *Epiplioptithecus* as a stem catarrhine, whereas the dashed line (B) denotes the alternative hypothesis that *Epiplioptithecus* would be more closely related to hominoids. Key nodes are highlighted as follows: gray circle = crown anthropoids; green circle = crown platyrrhines; blue circle = crown catarrhines; orange circle = crown hominoids. Skulls and crania (not to scale) were taken from the following sources for illustrative purposes only: extant skulls and *Aegyptopithecus*, Wikimedia Commons; *Dolichocebus*, Kay et al.

(2009b: Fig. 1); *Homunculus*, Tejedor and Rosenberger (2008: Fig. 2); *Oreopithecus* (reconstruction), Moyà-Solà and Köhler (2000: Fig. 5); *Epipliopithecus*, photograph of a cast; *Parapithecus*, digital reconstruction with photographic texture made by Steven Heritage.

2.4. Shape analysis

Differences in vestibule and SC shape were evaluated using a landmark-free 3DGM technique based on deformation, which relies on the geometrical correspondence of continuous surfaces and computes the magnitude and direction of deformation of the analyzed meshes from a group-average template (Glaunès and Joshi, 2006; Durrleman et al., 2012a, b; Dumoncel et al., 2014; Beaudet et al., 2016; Urciuoli et al., 2020). The deformations are mathematically modeled to obtain a one-to-one correspondence of the 3D space using the open-source software Deformetrica 4 (Bône et al., 2018). This technique yields results similar to landmark-based 3DGM methods while more easily tracking changes in volume (Urciuoli et al., 2020), and is less prone to biases introduced by the design of landmarking protocols, caused by the inherent difficulty to adequately capture complex 3D shapes based on a reduced number of homologous landmarks.

Due to the high computational power required, the sets of vectors, representing the flow of deformations from the initial position of the control points on the template to the target shape, were computed in the Barcelona Supercomputing Center (BSC) using the MinoTauro cluster (<https://www.bsc.es/marenostrum/minotauro>). To identify major patterns of shape variation across the sample, the resulting sets of vectors were inspected using between-group principal component analysis (bgPCA; Mitteroecker and Bookstein, 2011), using major clades (platyrrhines, cercopithecoids, hylobatids, and hominids) as the grouping factor (Urciuoli et al., 2020). To address recent concerns about the use of bgPCA based on highly multivariate data sets, such as those generated by 3DGM, and to rule out the presence of spurious groupings in our results (Bookstein, 2019; Cardini, et al., 2019),

we computed cross-validated bgPCA scores. These were obtained by iteratively repeating the bgPCA on a subset of the sample. The cross-validated bgPCA scores were then compared to those obtained with standard bgPCA (Cardini and Polly, 2020). The affinities of fossil specimens with the groups defined a priori in the bgPCA were evaluated using the 'typprobClass' function of the Morpho package v. 2.7 (Schlager, 2017) in R v. 3.6.1 (R Core Team, 2019). This function computes posterior probabilities of group membership based on the Mahalanobis distances between the bgPCA scores of fossil specimens and group centroids. Null hypotheses of group membership were rejected at $p < 0.05$.

Similarities among anthropoid species were also evaluated by running a cluster analysis (Ward's method) on the Mahalanobis distances between pairs of bgPCA species centroid scores using the 'ward.D2' method of the 'hclust' function of the 'stats' package in R. The cophenetic correlation coefficient, which allows one to evaluate how faithfully the obtained dendrogram preserves the pairwise distances between the original unmodeled datapoints, was calculated using the same package.

In addition, we inspected the volumetric proportions of *Epipliopithecus* and the remaining fossil taxa included in the analysis, and determined the correlation between log-transformed cube root canal volume (ln VolSC, mm) and log-transformed canal length (ln L, mm) by means of ordinary least-squares regression. Given that previous analyses identified an allometric grade shift between hominids and nonhominid anthropoids (Urciuoli et al., 2020), separate regression lines were computed for hominids and nonhominid anthropoid taxa using the 'stats' package in R.

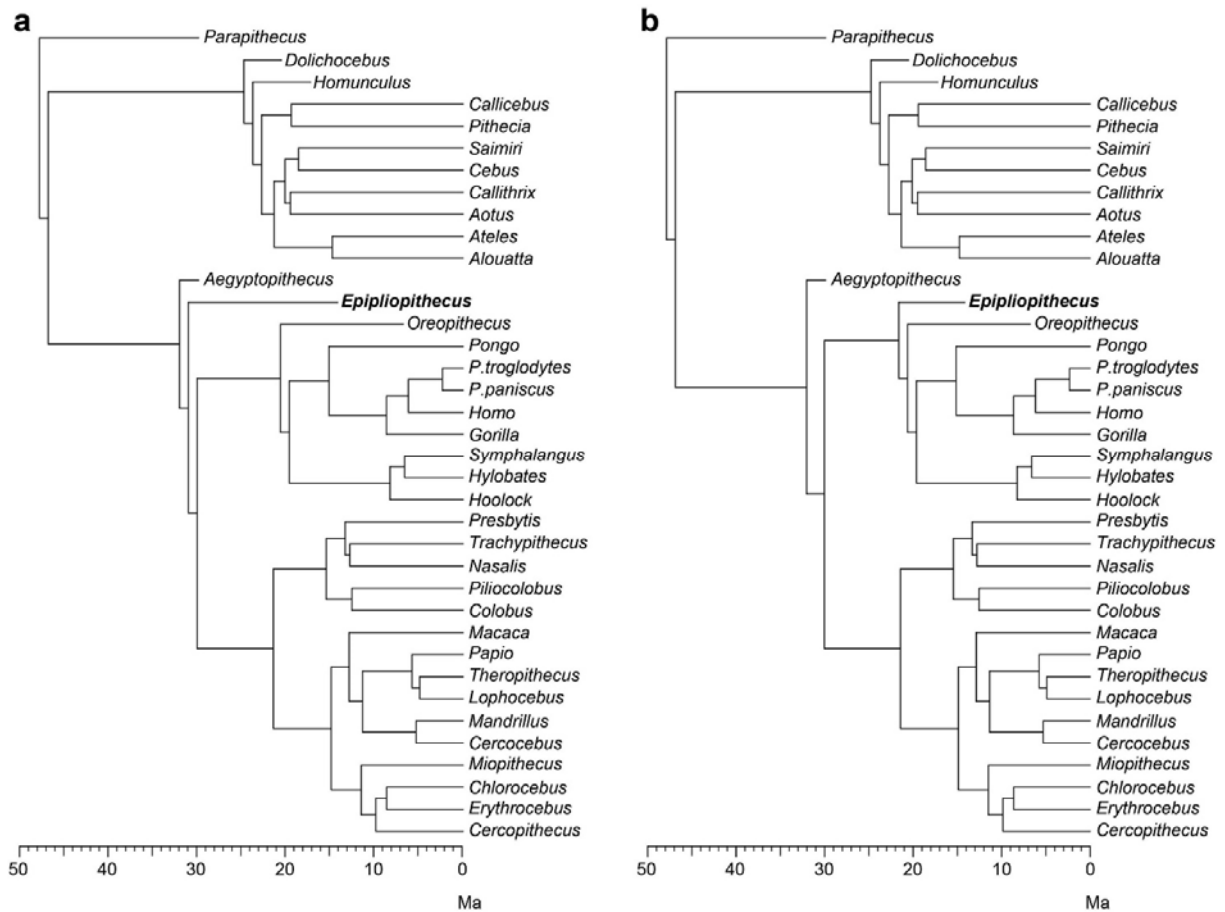


Figure 3. Phylogenetic trees used for the phylomorphospace approach. They differ in considering *Epiplioptithecus* as a stem catarrhine (a) or a stem hominoid (b).

2.5. Phylomorphospace, ancestral state estimation, and phylogenetic signal

To intuitively visualize the direction and magnitude of evolutionary change we relied on a phylomorphospace approach (Sidlauskas, 2008), by which a phylogenetic tree is projected onto the tangent space defined by the bgPCA of our shape data. Ancestral states for the internal nodes are estimated using a maximum likelihood method for continuous characters via the ‘fastAnc’ function of the ‘phytools’ version 0.6-60 package for R (Revell, 2012), while the tips of the tree branches correspond to the centroid scores for the included taxa. We repeated the analyses using two composite phylogenetic trees, one with *Epiplioptithecus* as a stem catarrhine and the other with this taxon as a stem hominoid (Figs. 2 and 3). For extant taxa we relied on a Bayesian phylogenetic analysis of

eleven mitochondrial and six autosomal genes downloaded from the 10kTrees Website v. 3 (Arnold et al., 2010). Extinct species were added based on their phylogenetic position, their divergence being arbitrarily placed 1 Myr before the estimated divergence age of the next derived node, and tip ages based on their chronostratigraphic age. We used the following tip age estimates: *Epipliopithecus* 14.15 Ma (mean of 14.85 and 13.45 Ma, the maximum-minimum age range for MN6 in central Europe according to van der Meulen et al., 2011); *Aegyptopithecus* and *Parapithecus*, 29.85 Ma (mean of 30.2 and 29.5 Ma, based on the revised age range of the fauna of quarries I and M of the Jebel Qatrani Formation of the Fayum depression by Seiffert, 2006); *Dolichocebus*, 20.5 Ma (mean of 21.0 and 20.0 Ma age provided by Kay, 2015); *Homunculus*, 17.2 Ma (mean of 17.9 and 16.5 Ma age provided by Kay, 2015); and *Oreopithecus* 6.75 Ma (mean of 7.0 and 6.5 Ma for the last occurrence according to Rook et al., 2000).

The phylogenetic signal embedded in the shape data was measured using Pagel's λ (Pagel, 1999) and Blomberg's K (Blomberg et al., 2003), together with the multivariate version of Blomberg's K (K_{mult} ; Adams, 2014). Pagel's λ and Blomberg's K were computed using the 'phylosig' function of the 'phytools' package in R, while K_{mult} was computed with the 'physignal' function of the 'geomorph' package v. 3.1.0 in R (Adams et al., 2019). These metrics were computed based on extant taxa only (Arnold et al., 2010).

Ancestral node morphologies were computed from the bgPC scores for the last common ancestors (LCAs) estimated by means of maximum likelihood, which were rotated and translated from the morphospace back into the deformation field space, generating a set of momentum vectors that were used in Deformetrica 4 to warp the template surface into the target LCA morphology. Volumetric proportions for the LCAs were computed based on the rescaled 3D models obtained from the phylomorphospace approach; the scaling factor for each LCA was estimated using the 'anc.ML' function of the R package 'phytools'. Morphological similarities between *Epipliopithecus* and the LCA

centroids were assessed by means Euclidean distances between the *Epipliopithecus* centroid and the LCA bgPC scores, weighted on the basis of the percentage of variance explained by each bgPC and computed using the ‘distances’ function of the ‘distances’ package version 0.1.8 in R (Savje, 2019).

The two phylogenetic hypotheses for *Epipliopithecus* depicted in Figure 3 were assessed further based on the coding of seven discrete characters that were deemed of phylogenetic significance based on shape comparisons and analyses. The resulting character-taxon matrix was analyzed for character congruence against a fixed topology consistent with the phylogenetic hypotheses depicted in Figure 3. For both cladograms, three indices customarily employed in cladistics (Farris, 1989) were computed in PAUP* v. 4.0a168 for Mac (Swofford, 2003) to assess the most parsimonious hypothesis: the consistency index (CI), the retention index (RI), and the rescaled consistency index (RC).

3. Results

3.1. Description and comparisons

The three bony labyrinths of *E. vindobonensis* are well preserved—except for the lateral canal of NMB OE 303b, which shows a small fracture in the bony encasing—and are not affected by diagenetic deformation, thereby permitting a straightforward extraction of the 3D surfaces of the vestibular apparatus bony labyrinth (Fig. 4a–c). Overall, the canals are fairly slender, as in platyrrhines and cercopithecins, falling within their variability as shown by a bivariate plot of SC volume vs. length (Fig. 5; Table 2; SOM Table S3). The bony vestibule is large, albeit less so than in hominids. The anterior and posterior canals are larger than the lateral canal, as in platyrrhines (Fig. 4e–i) and modern humans (Fig. 4u).

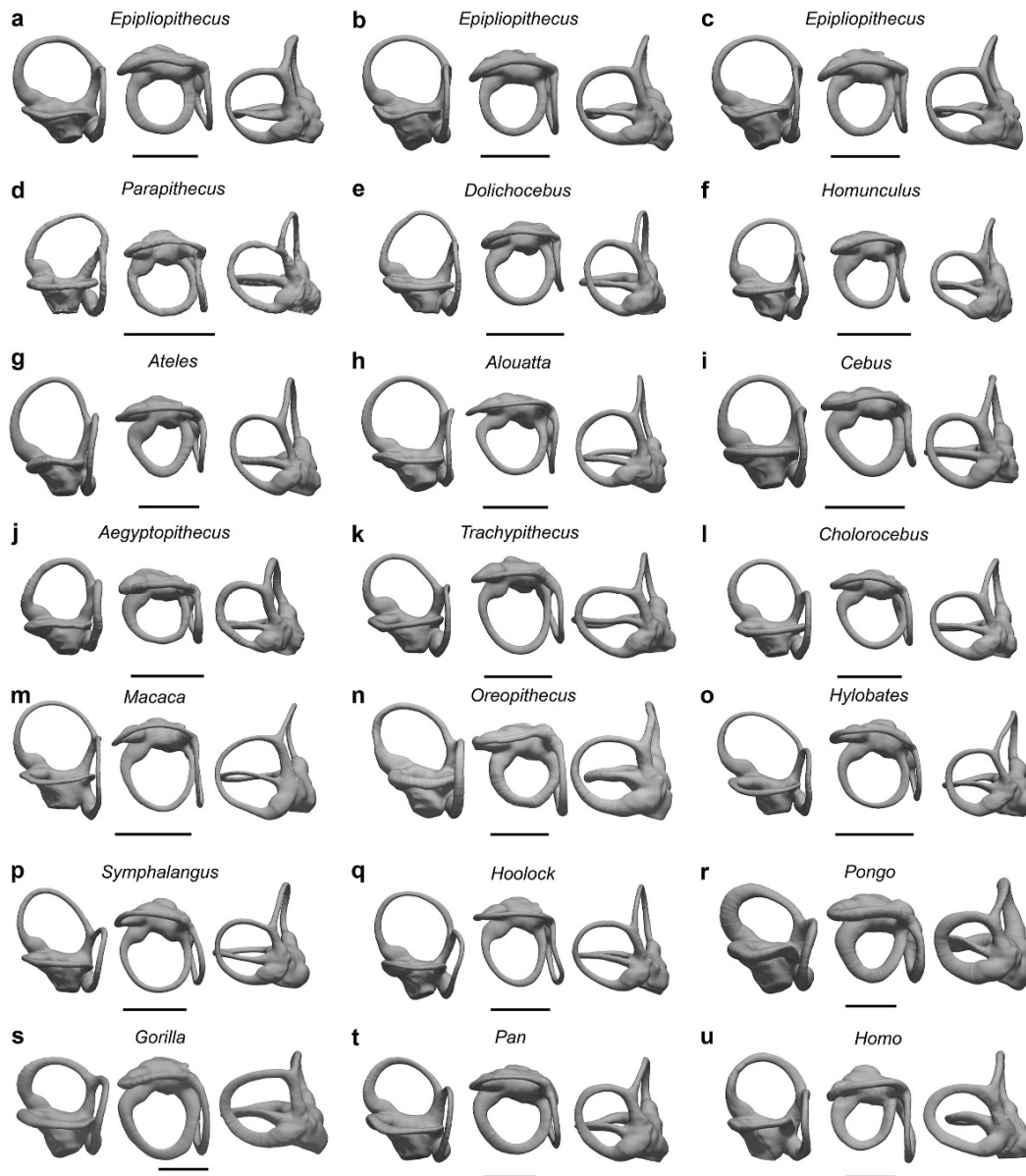


Figure 4. Rendered 3D models of the semicircular canals and vestibule of *Epipliothecus vindobonensis* (all specimens depicted as from the left side) and selected extant anthropoids, in lateral (left), superior (middle), and posterior (right) views: a) *E. vindobonensis* (individual II, NHMW 1970/1397/0003, mirrored); b) *E. vindobonensis* (individual III, NMB OE 303a); c) *E. vindobonensis* (individual III, NMB OE 303b, mirrored); d) *Parapithecus grangeri* (DPC 18651); e) *Dolichocebus gaimanensis* (MACN 14128); f) *Homunculus patagonicus* (MPM-PV 3501); g) *Ateles geoffroyi* (MCZ 29628); h) *Alouatta palliata* (DU EA LP12); i) *Cebus apella* (MCZ27891); j) *Aegyptopithecus zeuxis* (CGM 85785); k) *Trachypithecus cristatus* (MCZ35603); l) *Chlorocebus pygerythrus* (SIU 4796); m) *Macaca fascicularis* (MCZ 35765); n) *Oreopithecus bambolii* (BAC 208); o) *Hylobates lar* (MCZ 41424); p) *Symphalangus syndactylus* (AMNH.M 106583); q) *Hoolock hoolock* (AMNH.M 83425); r) *Pongo pygmaeus* (IPS10647); s) *Gorilla gorilla* (AMNH.M 167338); t) *Pan paniscus* (MCZ 38019); u) *Homo sapiens* (EMBR 179). Scale bars equal 5 mm.

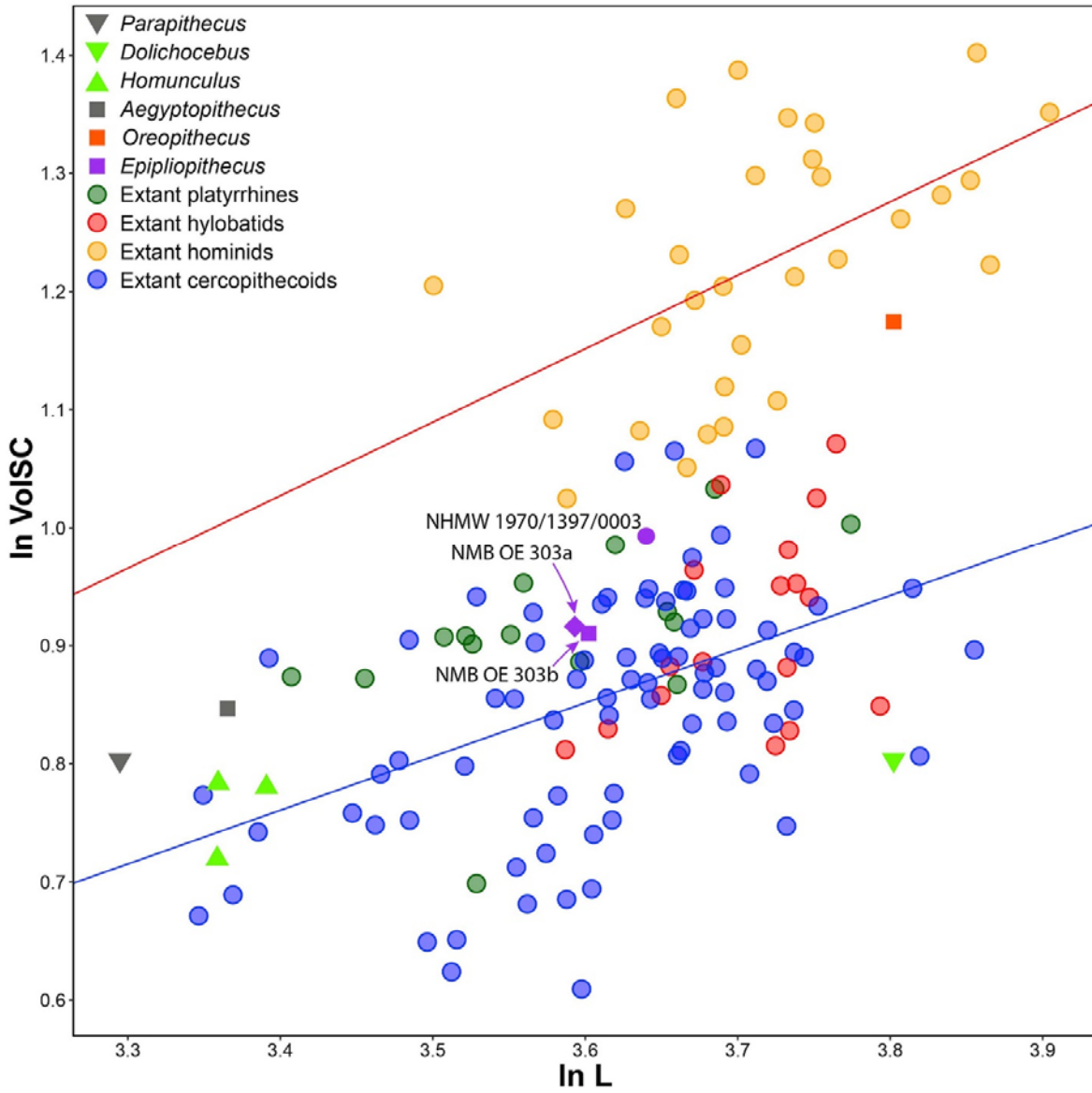


Figure 5. Bivariate plot of canal log-transformed cube root canal volume (mm; Ln VolISC) vs. log-transformed canal length (mm; Ln L). Separate regression lines are depicted for hominids (red line) and for nonhominid anthropoids (blue line). *Epiplioptithecus* (NHMW 1970/1397/0003 and NMB OE 303a, b) falls within the variability of nonhominid anthropoids, similar to all extinct taxa except *Oreopithecus*. Measurements for the included fossil taxa given in Table 6.

Table 2
Log-transformed cube root of canal volume (ln VolSC, mm³) and log-transformed canal length (ln L, mm) measured for the fossil taxa included in the analysis.^a

Catalog No.	Taxon	ln VolSC	ln L
NMBOE 303a	<i>Epipliopithecus vindobonensis</i>	3.640	0.993
NMBOE 303b	<i>Epipliopithecus vindobonensis</i>	3.602	0.910
NHMW 1970/1397/0003	<i>Epipliopithecus vindobonensis</i>	3.593	0.916
CGM 85785	<i>Aegyptopithecus zeuxis</i>	3.365	0.847
MPM-PV 30501	<i>Homunculus patagonicus</i>	3.391	0.780
MPM-PV 30502	<i>Homunculus patagonicus</i>	3.359	0.720
MPM-PV 30503	<i>Homunculus patagonicus</i>	3.359	0.784
MACN 14128	<i>Dolichocebus gaimanensis</i>	3.802	0.803
BAC 208	<i>Oreopithecus bambolii</i>	3.295	0.803
DPC 18651	<i>Parapithecus grangeri</i>	3.640	0.993

Abbreviations: BAC = Baccinello (field acronym; housed at Naturhistorisches Museum Basel, Switzerland); CGM = Egyptian Geological Museum, Cairo, Egypt; MPM-PV = Museo Regional Provincial Padre M.J. Molina, Río Gallegos, Argentina; MACN = Museo Argentino de Ciencias Naturales, Buenos Aires, Argentina; DPC = Duke Lemur Center, Durham, NC, USA.

^a See SOM Table S1 for the specimens included in the extant comparative sample.

The *E. vindobonensis* common crus (CC) is long, as in extant platyrrhines (Fig. 4g–i) and in *Dolichocebus* (Fig. 4e), but unlike in most catarrhines. The trajectories of the anterior and posterior canal form a right angle when merging at the CC apex. Despite some similarities, the morphology of *Epipliopithecus* is clearly distinguishable from that of *Dolichocebus* and *Parapithecus* (Fig. 4d), as the CC is not posteromedially inclined and the anterior canal connection is placed more laterally.

The anterior canal of *E. vindobonensis* is slightly wider than tall (as in *Hoolock*; Fig. 4q), yet clearly rounded and lacking the vertical compression characteristic of extant hominoids (Fig. 4o–u), the anterosuperior elongation typical of hylobatids and *Pongo* (Fig. 4o–r; Urciuoli et al., 2020), and the extreme superior projection found in *Ateles* (Fig. 4g). The anterior canal of *Epipliopithecus* further differs from that of the stem anthropoid *Parapithecus* (Fig. 4d), the stem platyrrhine *Dolichocebus* (Fig. 4e), and the stem catarrhine *Aegyptopithecus* (Fig. 4j), characterized by an almost triangular morphology (albeit less so in the last genus). The superiormost portion of the anterior canal bends medially, causing a moderate torsion of the canal trajectory. This morphology is also found in the stem platyrrhine *Homunculus* (Fig. 4f) and, to a lesser extent, *Chlorocebus* (Fig. 4l) and *Dolichocebus* (Fig. 4e), while in most cercopithecoids it is much more bent (e.g.,

Macaca; Fig. 4m). A sinuous trajectory of the anterior canal, although with a different morphology, is also displayed by other taxa (e.g., *Cebus*; Fig. 4i) and thus is not very informative from a phylogenetic viewpoint. Despite the aforementioned similarities, *Epipliopithecus* differs from the stem platyrrhines *Homunculus* (Fig. 4f) and *Dolichocebus* (Fig. 4e), from most extant platyrrhines (particularly *Ateles*; Fig. 4g), and from the stem catarrhine *Aegyptopithecus* (Fig. 4j), in displaying a much less mediolaterally compressed anterior canal.

The posterior canal of *Epipliopithecus* is slightly taller than wide, similar to that of *Alouatta* (Fig. 4h) and *Symphalangus* (Fig. 4p), but differs from the latter by displaying a less arched connection with the CC. The orientation of the posterior canal relative to the plane defined by the anterior canal is different in the two individuals of *Epipliopithecus*: it forms an obtuse angle in NHMW 1970/1397/0003 (resembling the hylobatid condition), but forms a right angle in NMB OE 303 (as in other anthropoids; SOM Fig. S2).

The lateral canal is rounded and smaller than the other canals (more so in NMB OE 303), as in stem platyrrhines (Fig. 4e, f) and the stem catarrhine *Aegyptopithecus* (Fig. 4j), although in *Epipliopithecus* this canal is not strongly compressed mediolaterally as in the latter taxon (Fig. 4j). The trajectory of the ampullary portion of the lateral canal slightly bends superiorly (more so in NMB OE 303; Fig. 4b, c), while the insertion of its slender part is located anteriorly to the base of the CC (particularly in NHMW 1970/1397/0003; Fig. 4a), so that—as in extant hominoids but unlike cercopithecoids—the lateral canal does not intersect the plane defined by the posterior canal. The lateral canal also shows a wave-like shape, with its lateral-most tip pointing downwards, superficially resembling some individuals of *Pongo* (Fig. 4r), while differing from the morphology of *Trachypithecus* (Fig. 4k) and *Macaca* (Fig. 4m), where the canal bends inferiorly right before the ampullary portion.

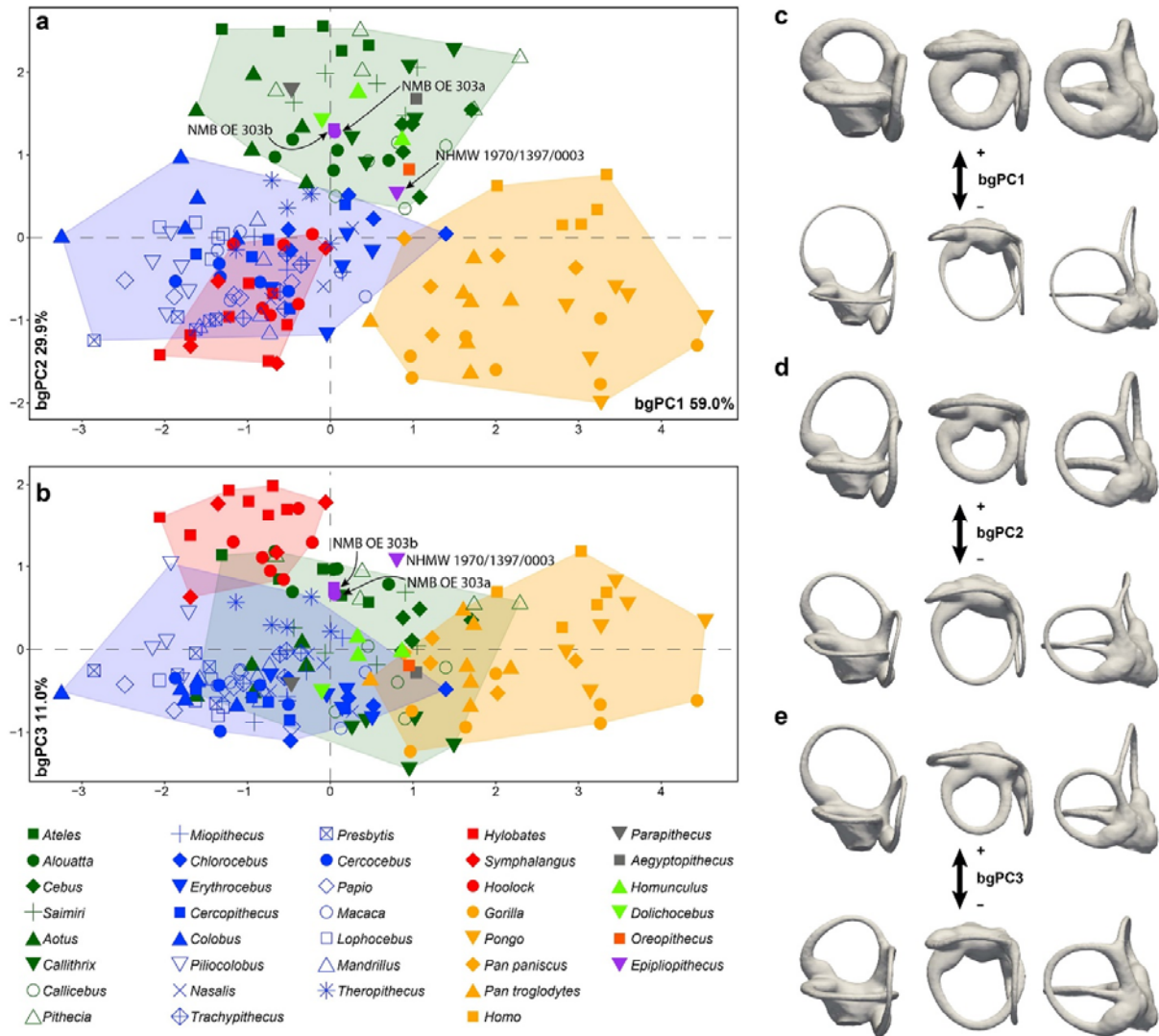


Figure 6. Patterns of vestibule and semicircular canal shape variation among major anthropoid clades based on the results of a between-group principal component analysis, as depicted by bivariate plots between principal components (bgPCs): a) bgPC2 vs. bgPC1; b) bgPC3 vs. bgPC1. Variance explained by each component is given along each axis. c–e) Extreme conformations of maximum (above) and minimum (below) bgPC scores: c) bgPC1; d) bgPC2; e) bgPC3. Four groups (platyrrhines, cercopithecoids, hylobatids, and hominids) were defined a priori, whereas specimens of *Epipliopithecus vindobonensis* were plotted post hoc onto the morphospace. Renderings in lateral (left), superior (middle), and posterior (right) views of warped 3D models representing the extreme conformations for each bgPC are placed close to the corresponding axis. Convex hulls depict the range of variation for a priori defined groups using the following color code: green = platyrrhines; blue = cercopithecoids; red = hylobatids; orange = hominids.

3.2. Shape analysis

The bgPCA discriminates major anthropoid clades with just minimal overlap when the three axes are considered simultaneously (Fig. 6), thus closely resembling the previous results by Urciuoli et al. (2020) despite the increased number of platyrrhine taxa included here. The bgPCA results reported in Figure 6 closely resemble those derived using a cross-validated bgPCA (SOM Fig. S1), indicating that group separation is not spurious (Cardini and Polly, 2020).

The first principal component (bgPC1, which explains 59% of the variance) mainly reflects differences in volumetric proportions among the SCs and the volume they occupy relative to that of the bony vestibule, separating hominids (stout canals; quite negative scores) from both cercopithecoids and hylobatids (slender canals; positive to slightly negative scores), while platyrrhines (including stem taxa), the stem anthropoid *Parapithecus*, the stem catarrhine *Aegyptopithecus*, the stem hominoid *Oreopithecus*, and *Epipliopithecus* occupy an intermediate position in the morphospace. In particular, the two *Epipliopithecus* individuals, due to their fairly slender canals (Fig. 4a–c), display similar intermediate scores along this axis, overlapping extensively with both extant and extinct platyrrhines in the overlap zone of cercopithecoids and hominoids (Fig. 6a, c).

In turn, bgPC2 (which explains 30% of the variance) accounts for differences in the size and shape of the anterior and posterior canals (Fig. 6a, d), in the position of the lateral canal ampullary insertion on the vestibule, and in CC length, separating most platyrrhines (positive scores) from catarrhines (moderately positive to negative scores). In particular, platyrrhines possess large and very superiorly elongated canals in the portion close to the CC apex, as well as a flat lateral canal, which also connects more inferiorly on the vestibule with its ampullary portion. Catarrhines are more variable in these features, showing rounded to vertically compressed anterior and posterior canals, a shorter CC, and a variably sinuous lateral canal with its ampullary portion connecting more superiorly.

Epipliopithecus displays moderately positive scores, falling within the range of several extant platyrrhines (*Aotus*, *Alouatta*, *Callithrix* and *Callicebus*), due to their large anterior and posterior canals, coupled with a long CC and a small lateral canal. Both the stem platyrrhines and *Oreopithecus* show similar moderately positive scores, while *Aegyptopithecus* and *Parapithecus* show markedly positive values due to their superiorly elongated vertical canals (Fig. 6a).

Finally, bgPC3 (which explains 11% of the variance) is driven by the position of the lateral canal relative to the posterior one, by the size and orientation of the posterior canal, as well as the shape of the anterior canal and CC thickness (Fig. 6b, e), separating hylobatids (most positive values) from most extant and fossil anthropoids (intermediate to negative scores). Hylobatids have a much larger gap between the lateral and posterior canals than other anthropoids except some modern humans, and their posterior canal is also smaller than, and forms an obtuse angle with, the large and anteriorly-protruding anterior canal. In contrast, in most cercopithecoids, *Aotus*, and *Callithrix*, the lateral canal broadly intersects with the posterior canal, while in the African great apes, *Theropithecus*, and *Cebus* the canals are only minimally separated. In addition, in all extant anthropoids except hylobatids, the plane of the posterior canal forms a right angle with the anterior canal, which does not project anteriorly. Both *Epipliopithecus* individuals display positive scores (NMB OE 303 with lower values), overlapping with some hylobatids (mainly *Hoolock*) and other extant anthropoids (particularly the hominids *Homo* and *Pongo*, the platyrrhines *Ateles* and *Alouatta*, and the cercopithecoids *Theropithecus* and *Ptilocolobus*). The slightly dissimilar bgPC3 scores for the two *Epipliopithecus* individuals result from differences in orientation between the posterior and anterior canals (obtuse angle in NHMW 1970/1397/0003 vs. right angle in NMB OE 303; SOM Fig. S2), causing a wider separation between the lateral and posterior canals (Fig. 4a–c).

When the three bgPCs are considered together, the two *Epipliopithecus* individuals show the greatest morphological similarities with platyrrhines (less so in NHMW 1970/1397/0003), as demonstrated by Mahalanobis distances from group centroids and by their posterior probabilities of group membership (Table 3), leading us to reject close similarities to the remaining groups for NMB OE 303, and to all anthropoid groups for NHMW 1970/1397/0003 ($p < 0.05$). *Aegyptopithecus*, *Parapithecus*, *Oreopithecus*, and stem platyrrhines also closely resemble extant New World monkeys, with *Oreopithecus* also showing marginal affinities with cercopithecoids (Table 3). We obtain very similar results when considering all catarrhines as a single group, with all fossils being classified as platyrrhines (Table 4). For *Oreopithecus* and NHMW 1970/1397/0003, group membership for catarrhines cannot be rejected. However, both specimens show much lower Mahalanobis distances to the platyrrhine centroid (almost three times) than to that of catarrhines. The two *Epipliopithecus* individuals are closer to one another than they are to other fossil taxa (except for one individual of *Homunculus*, MPM-PV 3501), in turn showing similarities with stem platyrrhines, *Aegyptopithecus* and *Oreopithecus* (Table 5). A cluster analysis based on the momenta of the deformation fields confirms these results (Fig. 7). *Epipliopithecus* clusters with *Alouatta* and *Ateles* (large and rounded vertical canals and a large gap between the lateral and posterior canals), as well as *Pithecia* (obtuse angle formed by the anterior and posterior canals), within a larger cluster that includes the remaining extant platyrrhines and the other fossil taxa included in the analysis. In particular, *Aegyptopithecus* and *Homunculus* cluster with *Saimiri* and *Cebus* (flat lateral canal and similarities in the anterior canal morphology), while *Oreopithecus* clusters with *Callicebus* (orientation of the anterior and posterior canals). Hylobatids cluster within a larger group that also includes most cercopithecoids, and extant great apes cluster together due to their distinctive stout volumetric proportions (Urciuoli et al., 2020).

Table 3

Mahalanobis distances (D^2) and posterior probabilities of group membership (p) based on the scores for fossil specimens in the between-group principal component analysis for the entire anthropoid sample.^{a,b}

D^2	Cercopithecoidea	Hominidae	Hylobatidae	Platyrrhini
<i>Epipliothecus vindobonensis</i> (NHMW 1970/1397/0003)	17.179	10.539	6.485	3.437
<i>Epipliothecus vindobonensis</i> (NMB OE 303a)	12.190	14.262	6.588	0.779
<i>Epipliothecus vindobonensis</i> (NMB OE 303b)	13.307	15.085	6.682	1.056
<i>Oreopithecus bambolii</i> (BAC 208)	8.083	5.450	11.574	1.579
<i>Aegyptopithecus zeuxis</i> (CGM 85785)	12.430	9.133	15.513	0.990
<i>Homunculus patagonicus</i> (MPM-PV 3501)	11.817	13.356	11.017	0.073
<i>Homunculus patagonicus</i> (MPM-PV 3502)	10.336	12.736	12.056	0.165
<i>Homunculus patagonicus</i> (MPM-PV 3503)	10.083	7.449	11.284	0.590
<i>Dolichocebus gaimanensis</i> (MACN 14128)	5.204	13.516	12.687	1.935
<i>Parapithecus grangeri</i> (DPC 18651)	6.533	17.859	13.047	2.110
P	Cercopithecoidea	Hominidae	Hylobatidae	Platyrrhini
<i>Epipliothecus vindobonensis</i> (NHMW 1970/1397/0003)	0.006	0.007	0.018	0.029
<i>Epipliothecus vindobonensis</i> (NMB OE 303a)	0.018	<0.001	<0.001	0.678
<i>Epipliothecus vindobonensis</i> (NMB OE 303b)	0.013	<0.001	<0.001	0.608
<i>Oreopithecus bambolii</i> (BAC 208)	0.052	0.005	<0.001	0.530
<i>Aegyptopithecus zeuxis</i> (CGM 85785)	0.001	<0.001	<0.001	0.688
<i>Homunculus patagonicus</i> (MPM-PV 3501)	0.003	<0.001	<0.001	0.980
<i>Homunculus patagonicus</i> (MPM-PV 3502)	0.003	<0.001	<0.001	0.919
<i>Homunculus patagonicus</i> (MPM-PV 3503)	0.019	0.001	<0.001	0.848
<i>Dolichocebus gaimanensis</i> (MACN 14128)	0.013	<0.001	<0.001	0.612
<i>Parapithecus grangeri</i> (DPC 18651)	0.002	<0.001	<0.001	0.411

Abbreviations: NHMW = Naturhistorisches Museum of Wien, Austria; NMB = Naturhistorisches Museum of Basel, Switzerland; BAC = NMB accession number for *Oreopithecus bambolii* specimens; CGM = Egyptian Geological Museum, Cairo, Egypt; MPM-PV = Museo Regional Provincial Padre M.J. Molina, Río Gallegos, Argentina; MACN = Museo Argentino de Ciencias Naturales, Buenos Aires, Argentina; DPC = Duke Lemur Center, Durham, NC, USA.

^a Note that these are probability estimates of having a particular score given membership in a particular group, not the likelihood of group membership in each of the a priori defined groups given a particular score (the greater the number, the higher the probability).

^b The lowest distance (D^2) and highest posterior probability of group membership (p) for each specimen are bolded.

Table 4

Mahalanobis distances (D^2) and posterior probabilities of group membership (p) based on the scores for fossil specimens in the between-group principal component analysis for the entire anthropoid sample and considering all catarrhines as a single group.^{a,b}

D^2	Catarrhini	Platyrrhini
<i>Epipliothecus vindobonensis</i> (NHMW 1970/1397/0003)	13.016	5.341
<i>Epipliothecus vindobonensis</i> (NMB OE 303a)	11.837	1.654
<i>Epipliothecus vindobonensis</i> (NMB OE 303b)	13.040	2.098
<i>Oreopithecus bambolii</i> (BAC 208)	9.085	3.890
<i>Aegyptopithecus zeuxis</i> (CGM 85785)	16.900	3.204
<i>Homunculus patagonicus</i> (MPM-PV 3501)	13.814	0.135
<i>Homunculus patagonicus</i> (MPM-PV 3502)	13.057	0.284
<i>Homunculus patagonicus</i> (MPM-PV 3503)	10.989	1.806
<i>Dolichocebus gaimanensis</i> (MACN 14128)	8.645	2.417
<i>Parapithecus grangeri</i> (DPC 18651)	12.592	3.670
P	Catarrhini	Platyrrhini
<i>Epipliothecus vindobonensis</i> (NHMW 1970/1397/0003)	0.109	0.241
<i>Epipliothecus vindobonensis</i> (NMB OE 303a)	0.022	0.876
<i>Epipliothecus vindobonensis</i> (NMB OE 303b)	0.017	0.847
<i>Oreopithecus bambolii</i> (BAC 208)	0.124	0.673
<i>Aegyptopithecus zeuxis</i> (CGM 85785)	0.002	0.886
<i>Homunculus patagonicus</i> (MPM-PV 3501)	0.002	0.985
<i>Homunculus patagonicus</i> (MPM-PV 3502)	0.002	0.968
<i>Homunculus patagonicus</i> (MPM-PV 3503)	0.034	0.935
<i>Dolichocebus gaimanensis</i> (MACN 14128)	0.013	0.841
<i>Parapithecus grangeri</i> (DPC 18651)	0.002	0.795

Abbreviations: NHMW = Naturhistorisches Museum of Wien, Austria; NMB = Naturhistorisches Museum of Basel, Switzerland; BAC = NMB accession number for *Oreopithecus bambolii* specimens; CGM = Egyptian Geological Museum, Cairo, Egypt; MPM-PV = Museo Regional Provincial Padre M.J. Molina, Río Gallegos, Argentina; MACN = Museo Argentino de Ciencias Naturales, Buenos Aires, Argentina; DPC = Duke Lemur Center, Durham, NC, USA.

^a Note that these are probability estimates of having a particular score given membership in a particular group, not the likelihood of group membership in each of the a priori defined groups given a particular score (the greater the number, the higher the probability).

^b The lowest distance and highest probability for each specimen are bolded.

Table 5Mahalanobis distances (D^2) between specimens of *Epipliothecus* and other fossils based on between group principal component analysis scores.

D^2	NHMW 1970/1397/0003	NMB OE 303a	NMB OE 303b
<i>Epipliothecus vindobonensis</i> (NHMW 1970/1397/0003)	–	1.332	1.285
<i>Epipliothecus vindobonensis</i> (NMB OE 303a)	1.332	–	0.176
<i>Epipliothecus vindobonensis</i> (NMB OE 303b)	1.285	0.176	–
<i>Oreopithecus bambolii</i> (BAC 208)	2.244	1.901	2.055
<i>Aegyptopithecus zeuxis</i> (CGM 85785)	2.360	1.804	1.927
<i>Homunculus patagonicus</i> (MPM-PV 3501)	1.943	0.919	1.033
<i>Homunculus patagonicus</i> (MPM-PV 3502)	2.246	1.251	1.388
<i>Homunculus patagonicus</i> (MPM-PV 3503)	1.914	1.450	1.592
<i>Dolichocebus gaimanensis</i> (MACN 14128)	3.081	2.077	2.243
<i>Parapithecus grangeri</i> (DPC18651)	3.201	2.017	2.161

Abbreviations: NHMW = Naturhistorisches Museum Wien, Austria; NMB OE = Naturhistorisches Museum Basel, Switzerland; BAC = Baccinello (housed at NMB); CGM = Egyptian Geological Museum, Cairo, Egypt; MPM-PV = Museo Regional Provincial Padre M.J. Molina, Rio Gallegos, Argentina; MACN = Museo Argentino de Ciencias Naturales, Buenos Aires, Argentina; DPC = Duke Lemur Center, Durham, NC, USA.

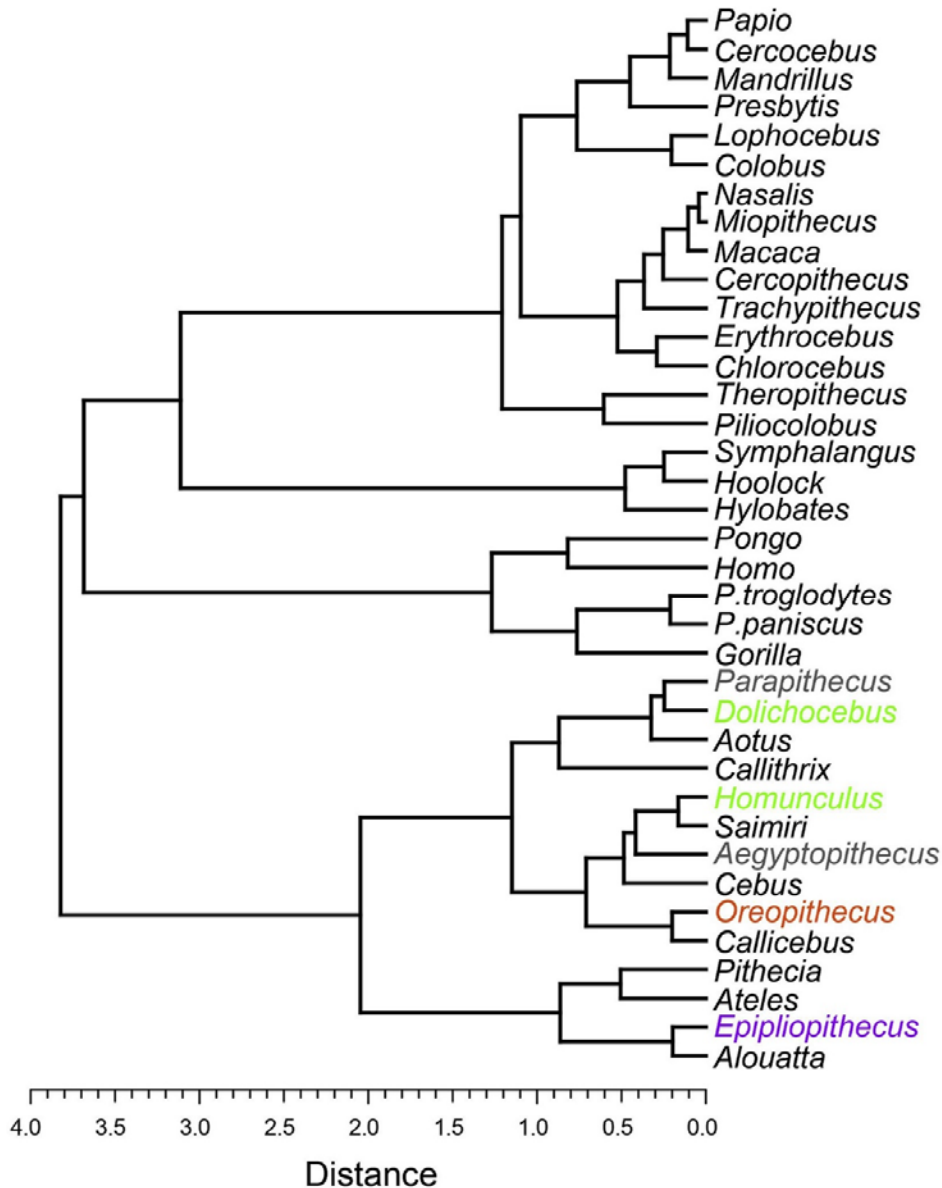


Figure 7. Dendrogram resulting from a cluster analysis (Ward's method) based on Mahalanobis distances computed between the species centroids of the between-group principal component analysis (bgPCA) of shape data. The cophenetic correlation coefficient is 0.703.

3.3. Phylogenetic signal and phylomorphospace

Like previous analyses (Urciuoli et al., 2020; del Rio et al., 2020; Morimoto, et al., 2020), our results indicate that the vestibule and SCs embed significant phylogenetic signal ($K_{\text{mult}} = 1.134$, $p < 0.001$), suggesting these traits conform to a Brownian motion model of evolution, with closely related taxa resembling one another slightly more than expected ($K_{\text{mult}} > 1$). The phylogenetic signal computed for each bgPC separately is significant in all instances (Table 6), with bgPC1 and bgPC2 suggesting the same evolutionary mode as K_{mult} ($K > 1$). Conversely, we observe that the variance accumulates within clades for bgPC3 ($K < 1$), thus suggesting that changes along this axis might be more strongly affected by homoplasy.

Table 6

Phylogenetic signal computed for the between-group principal analysis applied to the deformation fields of the extant anthropoid comparative sample. The variance explained by each principal component (bgPC) and the p -value for the statistics are given within parentheses.

	bgPC1 (59%)	bgPC2 (30%)	bgPC3 (11%)
Pagel's λ	1.000 ($p < 0.0001$)	0.843 ($p < 0.0001$)	0.925 ($p < 0.0001$)
Blomberg's K	1.148 ($p < 0.0001$)	1.446 ($p < 0.001$)	0.732 ($p < 0.001$)

The phylogenetic signal detected justifies the application of the phylomorphospace approach (Fig. 8). The results indicate that the reconstructed LCAs of crown anthropoids (Fig. 9a) and crown catarrhines (Fig. 9c) fall within the variability of extant New World monkeys, being very close to the platyrrhine LCA (Fig. 9b)—irrespective of the phylogenetic hypothesis used in the analysis for *Epipliothecus* (i.e., stem catarrhine vs. stem hominoid, Figs. 3 and 8; SOM Fig. S3). Cercopithecoids and hominoids appear much more derived in SC morphology than platyrrhines, but in different directions. The crown anthropoid, crown platyrrhine and crown catarrhine LCAs are reconstructed as possessing large and slightly vertically-elongated canals (more so in the crown anthropoid and crown platyrrhine LCAs; Fig. 9a, b) coupled with a long CC (shorter in the crown catarrhine LCA; Fig. 9c), intermediate volumetric proportions (similar to those found in New World monkeys

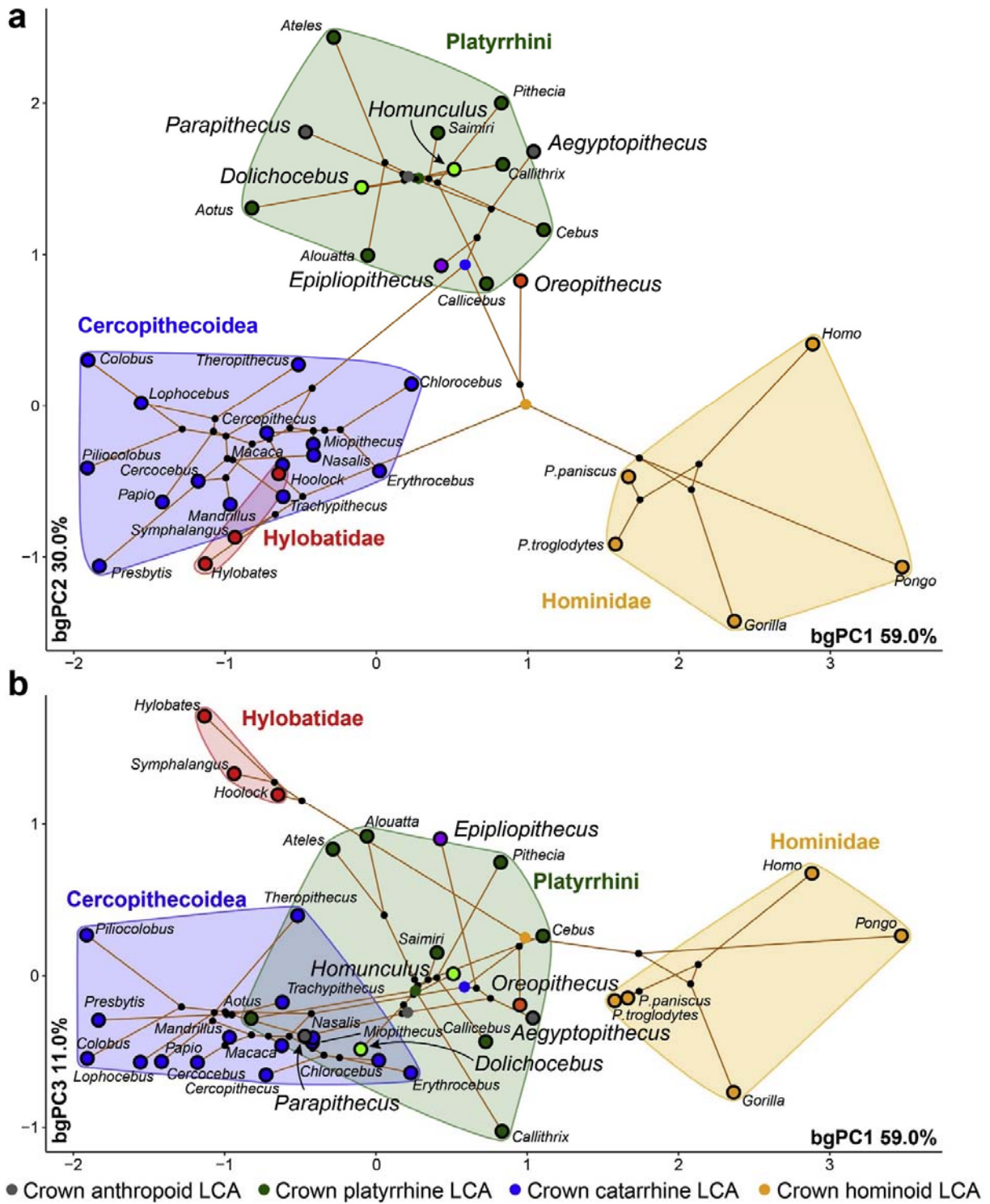


Figure 8. Phylomorphospace of the anthropoid semicircular canal. The phylogenetic tree (with *Epipliopithecus* included as a stem catarrhine; Fig. 3a) is projected onto the tangent space defined by the between-group principal components (bgPCs) as depicted in Figure 6. The internal nodes (i.e., the ancestral states) were estimated using maximum likelihood: a) bgPC2 vs. bgPC1; b) bgPC3 vs. bgPC1. Variance explained by each component is given along each axis. Convex hulls depict the range of variation for a priori defined groups using the following color code: green = platyrrhines; blue =

cercopithecoids; red = hylobatids; orange = hominids. The ancestral nodes discussed for assessing *Epiplioptithecus* phylogenetic affinities do not change consistently in their position in the morphospace irrespective of the phylogenetic hypothesis used for their estimation (see SOM Fig. S3 for the alternative phylogenetic tree including *Epiplioptithecus* as a stem hominoid). Key nodes are highlighted as follows: gray circle = crown anthropoids; green circle = crown platyrrhines; blue circle = crown catarrhines; orange circle = crown hominoids.

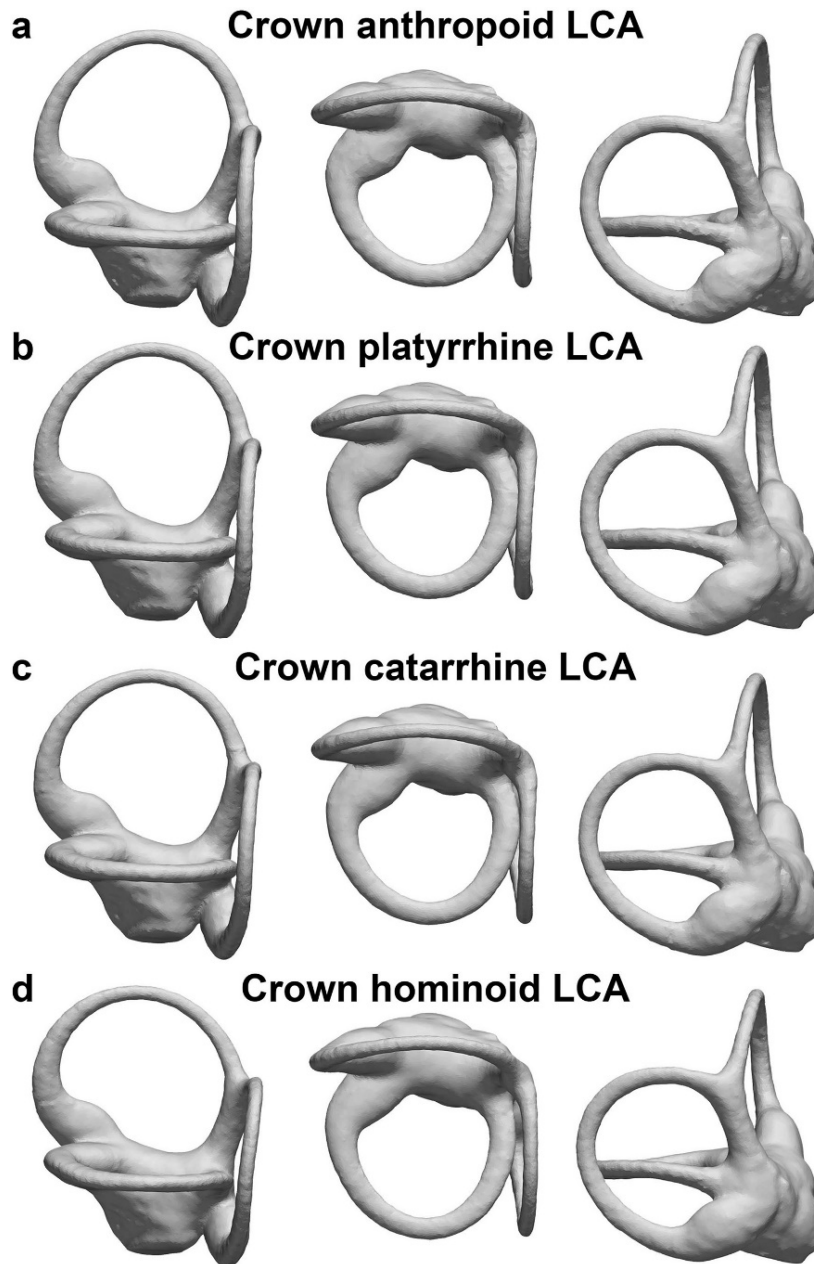


Figure 9. Reconstruction of the semicircular canals and vestibule for the last common ancestors (LCAs) of the following clades: a) crown anthropoids; b) crown platyrrhines; c) crown catarrhines; d) crown hominoids. The renderings of each 3D model are depicted in lateral (left), superior (middle), and posterior (right) views.

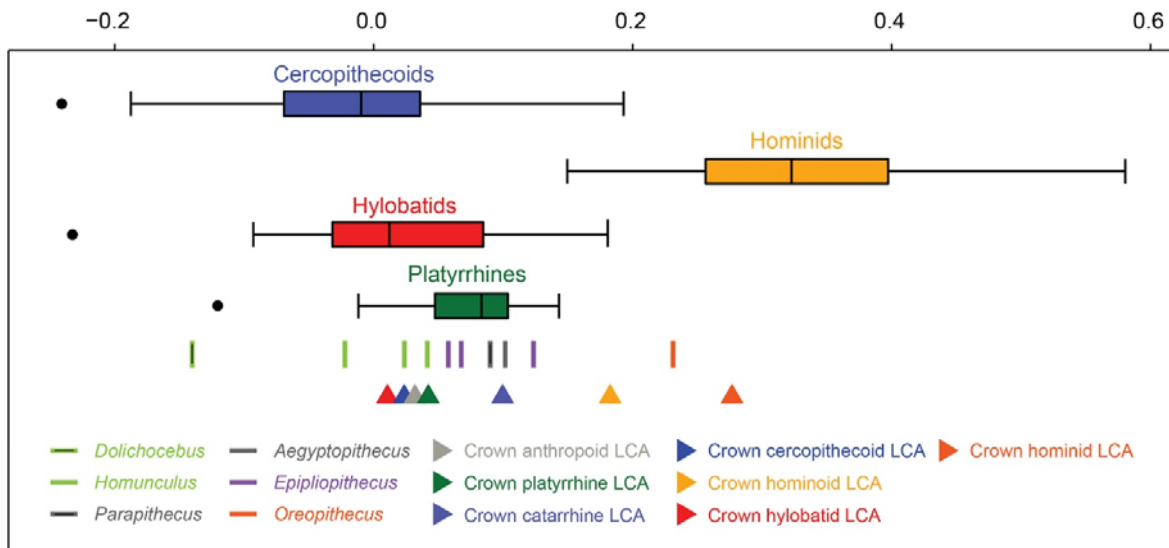


Figure 10. Box-and-whisker plot of allometric residuals based on best-fit line of the nonhominid anthropoid regression of log-transformed cube root of canal volume and log-transformed canal length (as depicted in Fig. 5). Vertical lines correspond to the median, boxes depict interquartile range, whiskers represent maximum and minimum values within 1.5 times the interquartile range, and black dots are outliers. Sample sizes for extant groups are the following: Platyrrhini ($n = 40$), Cercopithecoidea ($n = 75$), Hylobatidae ($n = 17$), Hominidae ($n = 30$).

and cercopithecins; Fig. 10), and a coplanar lateral canal that does not intersect the plane of the posterior one (Fig. 9a–c). The LCA of crown catarrhines also shows a slightly more superiorly bent ampullary portion, more so than in *Epipliopithecus* (Fig. 9c). In contrast, the reconstructed crown hominoid LCA (Fig. 9d) is found in an area of the morphospace devoid of extant taxa and, according to our estimation, it already displayed some derived characters that are not found in *Epipliopithecus* (i.e., moderately vertically-compressed anterior canal, stouter canal proportions, lateral ampulla connecting more superiorly with the vestibule).

From a phenetic viewpoint, based on weighted Euclidean distances between *Epipliopithecus* and the bgPC scores for the reconstructed LCAs (Table 7), the former taxon is most similar to the crown catarrhine ancestral condition, and also closer to the crown anthropoid and platyrrhine LCAs, than to the ancestral conditions reconstructed for either hominoids or cercopithecoidea.

Table 7

Weighted Euclidean distances computed between the between-group principal component scores of the reconstructed last common ancestors (LCAs) and the *Epipliopithecus* centroid.

LCA	Distance
Crown anthropoids	1.304
Crown platyrrhines	1.141
Crown catarrhines	0.989
Crown cercopithecoids	1.646
Crown hominoids	1.256

We further synthesized the information provided by the phylomorphospace approach by defining seven discrete characters coded in a cladistic fashion (Table 8; Fig. 11). Their coding for the reconstructed LCAs as well as both extant and extinct anthropoids included in the analyses is reported in Table 9 and SOM Table S4. When the character states for extinct and extant taxa are analyzed against the two phylogenetic hypotheses by considering parsimony as a criterion (Table 10), *Epipliopithecus* is more parsimoniously interpreted as a stem catarrhine (Fig. 3a) than as a stem hominoid (Fig. 3b). The phylogenetic implications of the seven coded characters (Fig. 11; Tables 8 and 9; SOM Table S4) are discussed below and illustrated in Figure 12.

Table 8

Definition of the discrete characters of semicircular canal (SC) and vestibule morphology used in this paper.

Character No.	Character statements (characters + character states) ^a
#1	Size of the vestibule relative to the SCs: 0 = small; 1 = large.
#2	Robusticity of the SCs: 0 = slender; 1 = stout.
#3	Shape of the anterior SC: 0 = vertically compressed; 1 = rounded; 2 = elongated superiorly.
#4	Shape of the anterior portion of the anterior SC: 0 = non-projecting anterosuperiorly; 1 = anterosuperiorly projecting.
#5	Shape of the posterior SC: 0 = vertically compressed; 1 = rounded; 2 = elongated superiorly.
#6	Shape of the lateral SC ampullary portion: 0 = flat or only slightly bent superiorly; 1 = markedly bent superiorly.
#7	Length of the CC: 0 = long; 1 = intermediate; 2 = short.

^a See Figure 11 for an illustration of the character states.

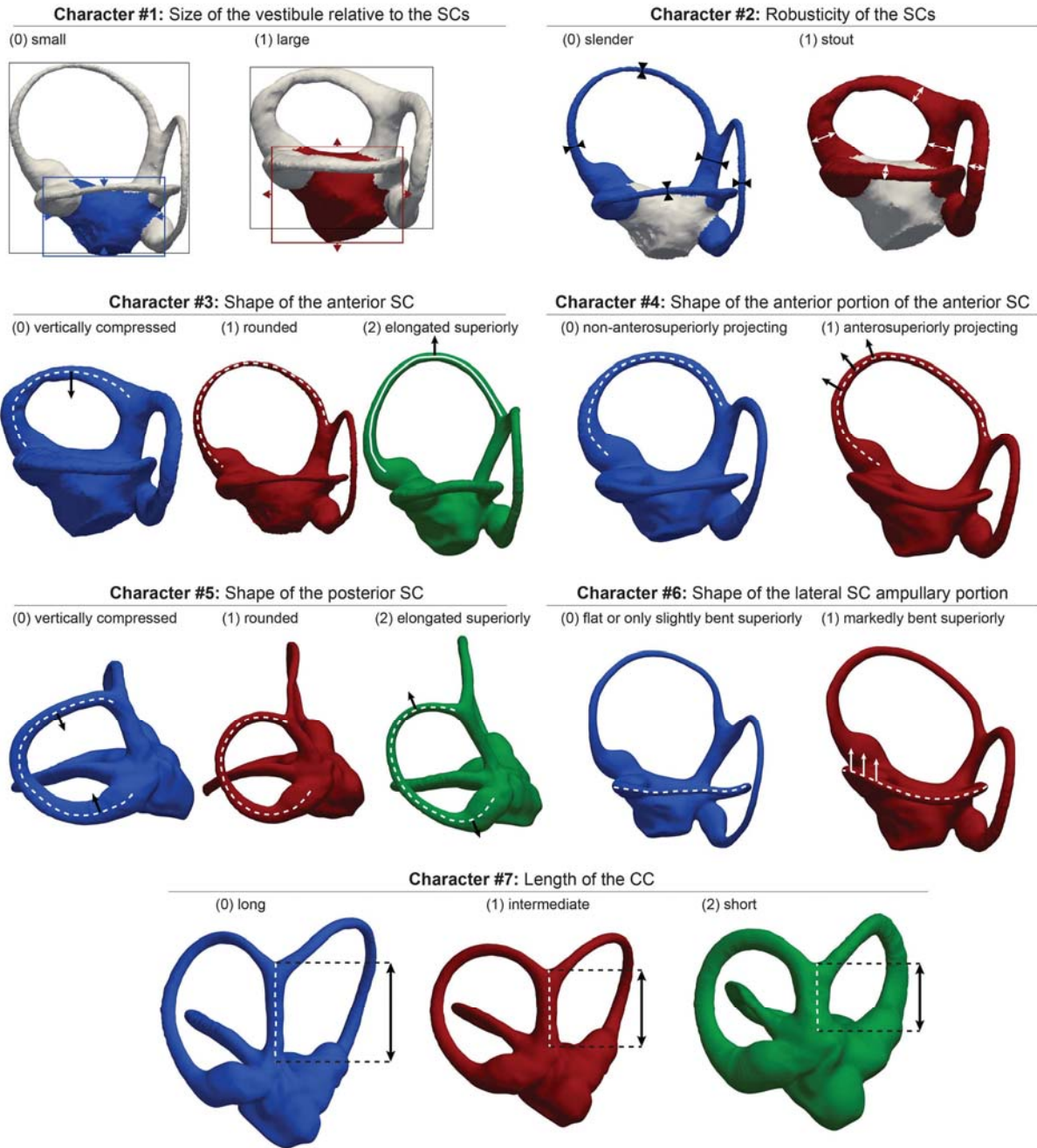


Figure 11. Illustration of the discrete characters of semicircular canal (SC) and vestibule morphology used in this paper. Numbers preceding each state (0, 1, 2) correspond to character states numbered in Tables 8 and 9, and SOM Table S4.

Table 9

Character states coded for the estimated last common ancestors (LCAs) and for the fossil taxa included in the analysis.^a

Species/LCAs	#1	#2	#3	#4	#5	#6	#7
<i>Epipliopithecus vindobonensis</i>	0	0	1	0	2	0	0
<i>Aegyptopithecus zeuxis</i>	0	0	2	0	2	0	0
<i>Dolichocebus gaimanensis</i>	0	0	2	0	2	0	0
<i>Homunculus patagonicus</i>	0	0	2	0	0, 2	0	0
<i>Oreopithecus bambolii</i>	1	1	0	1	1	0	2
<i>Parapithecus grangeri</i>	0	0	2	0	2	0	0
Crown anthropoid LCA	0	0	2	0	2	0	0
Crown platyrrhine LCA	0	0	2	0	2	0	0
Crown catarrhine LCA	0	0	1	0	1	0	1
Crown cercopithecoïd LCA	0	0	1	0	1	0	1
Crown hominoid LCA	0	0	0	0	1	1	2
Crown hylobatid LCA	0	0	0	1	1	1	2
Crown hominid LCA	1	1	0	0	1	1	2

^a See character definitions in Table 7 and SOM Table S2 for the coding of extant species.

Table 10

Measures of character congruence for the two main phylogenetic hypotheses (i.e., stem catarrhine vs. stem hominoid) discussed in this paper for *Epipliopithecus*. The higher the index, the more parsimonious the hypothesis.^a

Metrics	Stem catarrhine (Fig. 3a)	Stem hominoid (Fig. 3b)
Tree length	22	24
CI	0.455	0.417
RI	0.826	0.797
RC	0.376	0.332

Abbreviations: CI = consistency index; RI = retention index; RC = rescaled consistency index.

^a See also Figure 3 and SOM Table 2 for character descriptions.

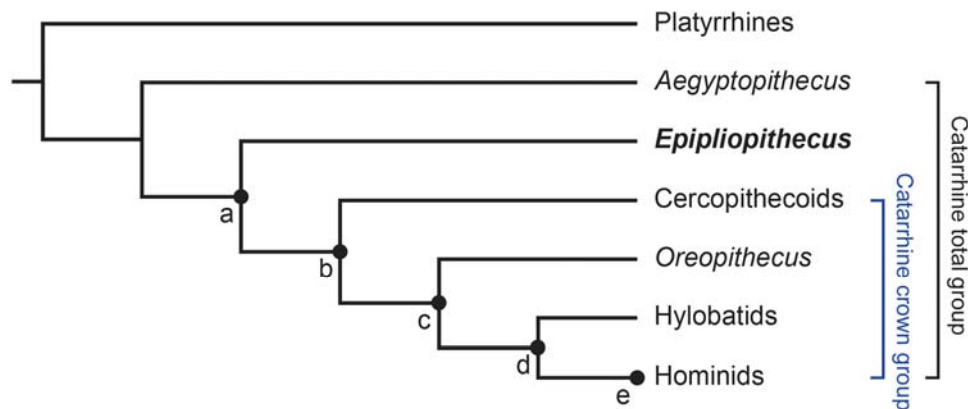


Figure 12. Simplified cladogram of crown anthropoids and selected extinct catarrhines (*Epipliopithecus* and *Oreopithecus*) summarizing the main synapomorphies inferred for the various clades in semicircular canal and vestibule morphology. The four extant anthropoid clades distinguished (platyrrhines, cercopithecoïds, hylobatids and hominids) are depicted as terminal nodes. The synapomorphies inferred for each node are summarized below; character number (preceded by a hash) and character state (within parentheses) are provided after each synapomorphy within brackets. a) *Epipliopithecus* + crown catarrhines: rounded anterior canal [#3(1)]; b) Crown catarrhines: rounded posterior canal

[#5(1)], moderately short CC [#7(1)]; c) *Oreopithecus* + crown hominoids: vertically compressed anterior canal [#3(0)], anterosuperiorly-projecting anterior portion of the anterior canal [#4(1)], short CC [#7(2)]; d) Crown hominoids: markedly superiorly bent ampullary portion of the lateral canal [#6(1)]; e) Crown hominoids (unless *Oreopithecus* + crown hominoid synapomorphies [node c] with reversal in hylobatids): large vestibule relative to the SCs [#1(1)], stout SCs [#2(1)]. Abbreviations: CC = common crus; SC = semicircular canals. See Figure 11 for an illustration of the various character states and Table 9 and SOM Table S4 for the scoring of reconstructed last common ancestors and individual taxa, respectively.

Size of the vestibule relative to the semicircular canals Extant hominids differ from all the remaining extant taxa in possessing a relatively larger vestibule, which may be thus interpreted as a synapomorphy of at least crown hominids. Among the extinct taxa, only the purported stem hominoid *Oreopithecus* displays the derived hominid condition, indicating either an independent acquisition of this feature in this taxon (as supported by our LCA reconstructions) or a secondary reversal in hylobatids. *Epipliopithecus*, in any case, retains the plesiomorphic condition of nonhominoid anthropoids.

Robusticity of the semicircular canals This character has the same distribution as the size of the vestibule relative to the SCs. Extant hominids and *Oreopithecus* differ from the remaining taxa by displaying stouter proportions. Accordingly, such proportions might be interpreted either as convergent between *Oreopithecus* and hominids, or as a hominoid synapomorphy with subsequent reversal in hylobatids. Our LCA reconstructions do not provide clear support for either possibility, as they suggest an intermediate ancestral condition in the overlap zone between hominoids and nonhominoid catarrhines. In either case, for this character *Epipliopithecus* displays the more plesiomorphic condition of nonhominoid anthropoids.

Shape of the anterior semicircular canal This character is more variable than the preceding ones, both within anthropoid subclades, and sometimes even within the same species. However, extant catarrhines generally differ from platyrrhines by possessing an anterior canal that is not superiorly elongated, being instead either rounded (as in humans

and most cercopithecoids) or vertically compressed (as in great apes and generally hylobatids, although in the latter it varies intraspecifically between rounded and vertically compressed). Our LCA reconstructions suggest that the ancestral anthropoid condition—a superiorly elongated anterior canal—is symplesiomorphic not only for platyrrhines but also for the stem catarrhine *Aegyptopithecus*. They further support the view that a rounded anterior SC is synapomorphic of crown catarrhines, while a vertically compressed anterior SC would be synapomorphic for crown hominoids + *Oreopithecus*. In this regard, *Epipliopithecus* is more derived than *Aegyptopithecus* but less so than *Oreopithecus*. This character, therefore, unambiguously supports for *Epipliopithecus* a catarrhine status more derived than in *Aegyptopithecus*, although it would be consistent with either a stem catarrhine or a stem hominoid status.

Shape of the anterior portion of the semicircular canal Hylobatids and orangutans differ from the rest of the sample by displaying an anterosuperiorly-projecting anterior portion of the anterior canal. This condition may be interpreted as a crown hominoid synapomorphy subsequently reversed in hominines, as further supported by the fact that *Oreopithecus* displays the derived condition for hominoids. Alternatively, this feature might have been independently acquired in *Oreopithecus*, as suggested by our LCA reconstructions, which only recover it as a hylobatid synapomorphy. Given the possession of other SC hominoid synapomorphies in *Oreopithecus*, we tend to favor the former interpretation, even if both are equally parsimonious. In any case, *Epipliopithecus* retains the more plesiomorphic condition of non-hominoid anthropoids.

Shape of the posterior semicircular canal Although this character is somewhat variable within anthropoid subclades and sometimes even within species, some generalities can be drawn. In platyrrhines, the posterior canal is generally elongated superiorly to some extent, whereas most cercopithecoids have a rounded posterior canal, and hominoids generally vary between a rounded and a vertically compressed morphology (only sometimes

superiorly elongated in *Pan*). Our LCA reconstructions indicate that platyrrhines and *Aegyptopithecus* retain the ancestral anthropoid condition (superiorly elongated posterior canal), whereas the rounded morphology would be synapomorphic for crown hominoids. *Epipliopithecus* displays the plesiomorphic anthropoid condition and thus differs from *Oreopithecus*, which displays the derived catarrhine morphology.

Shape of the lateral semicircular canal ampullary portion Extant hominoids differ from the remaining extant taxa and all the analyzed extinct genera by displaying a markedly superiorly-bent ampullary portion of the lateral canal. Both *Epipliopithecus* and *Oreopithecus* thus display a more plesiomorphic condition than crown hominoids, as further confirmed by our LCA reconstructions.

Length of the common crus This character is also variable to some extent, but platyrrhines generally display a longer CC than extant catarrhines, with hominoids having an even shorter CC than most cercopithecoids. Our LCA reconstructions support an intermediate length of the CC as synapomorphic of crown catarrhines, with a short CC being synapomorphic for hominoids. *Epipliopithecus* resembles *Aegyptopithecus* and platyrrhines by retaining the ancestral anthropoid condition, whereas *Oreopithecus* displays the derived hominoid morphology.

4. Discussion

Our analysis of the SC and vestibule morphology of *Epipliopithecus* allows us to refine our understanding of the evolution of this anatomical region in anthropoid primates and to refine previous hypotheses proposed by Urciuoli et al. (2020). The results of our deformation-based 3DGM analysis and the reconstruction of ancestral morphotypes for main anthropoid clades indicate that, like the stem catarrhine *Aegyptopithecus*, *Epipliopithecus* displays a platyrrhine-like morphology most similar to that reconstructed for the crown catarrhine LCA. This might be compatible with *Epipliopithecus* being either a

stem catarrhine, or a crown catarrhine only slightly postdating the cercopithecoid-hominoid split. However, the fact that *Epipliopithecus* most closely resembles the crown anthropoid (and platyrrhine) LCAs (Table 7) suggests that the semicircular morphology of this taxon is most consistent with its status as a stem catarrhine. This conclusion is further supported by the analysis of seven discrete characters coded for this anatomical area—which indicate that this is the most parsimonious hypothesis, for reasons discussed in greater detail below.

4.1. *Epipliopithecus* as a hominoid

Based on the morphology of the SCs and vestibule, *Epipliopithecus* lacks multiple hominoid synapomorphies, including a large vestibule relative to the canals, stout SCs, vertically-compressed anterior canal, anterosuperiorly- projecting anterior portion of the anterior canal, markedly superiorly-bent ampullary portion of the lateral canal, and short CC. Urciuoli et al.(2020) already interpreted some of these features (vertically-compressed anterior canal and markedly superiorly-bent ampullary portion of the lateral canal) as potential crown hominoid synapomorphies, whereas they interpreted others (large vestibule and stout canals) as hominid synapomorphies. Urciuoli et al. (2020) interpreted a superiorly-bent ampullary portion of the lateral canal as a hominoid synapomorphy. However, hominoids are, in fact, characterized by the possession of a markedly bent trajectory, whereas other catarrhines display a flat to slightly superiorly-bent ampullary portion of the lateral canal. This is the case for *Epipliopithecus*, which displays much less bending of the lateral canal than in *Oreopithecus* or any extant hominoid.

The possession of a large vestibule and stout canals was previously interpreted as being synapomorphic for hominids (Urciuoli et al., 2020) because hylobatids display a different ('monkey-like') condition. The differences in volumetric proportions between *Epipliopithecus* and hominids are particularly clear (Fig. 10), with the former closely

resembling platyrrhines, *Aegyptopithecus*, and the inferred ancestral catarrhine condition. Given that both features are present in *Oreopithecus*, they may be interpreted as hominoid synapomorphies subsequently reversed in hylobatids—thereby supporting a more basal branching for *Epipliopithecus*. However, their interpretation as hominoid synapomorphies is equally parsimonious, as it would only imply their independent acquisition in *Oreopithecus*. Therefore, neither a large vestibule nor stout canals can be used to unambiguously discount a hominoid status for *Epipliopithecus*. A similar caveat applies to the lack of an anterosuperiorly-projecting anterior canal in *Epipliopithecus*. This condition was previously interpreted as an autapomorphy of *Hylobates* (Le Maître, et al., 2017) or as a hylobatid synapomorphy (Spoor and Zonneveld, 1998; Urciuoli, et al. 2020). However, given its presence in orangutans and *Oreopithecus*, it is more readily interpreted as a hominoid synapomorphy subsequently reversed in hominines. The interpretation of some of the potential hominoid synapomorphies lacking in *Epipliopithecus* is ambiguous due to homoplasy (convergence and/or reversal). However, it is worth noting that, except for the markedly superiorly bent ampullary portion of the lateral canal, *Oreopithecus* further displays two more unambiguous hominoid synapomorphies (vertically compressed anterior canal and short CC). The absence of these features in *Epipliopithecus* thus conclusively excludes a more derived hominoid status for the latter as compared with *Oreopithecus*.

Epipliopithecus also displays some hylobatid-like features in the spatial configuration between the lateral and posterior canals, as well as in the orientation between the anterior and posterior canals. According to Urciuoli et al. (2020), the lack of intersection between the lateral and posterior canals and the presence of an obtuse angle between the anterior and posterior canals would be synapomorphic for hominoids and hylobatids, respectively. However, only *Hylobates* consistently displays both features, while most anthropoid taxa, as well as the two *Epipliopithecus* individuals, show a considerable amount of intraspecific variation. Hence, we refrained from coding these

features in a cladistic manner, especially in view of the low phylogenetic signal ($K < 1$) recovered for bgPC3 (accounting for the variation in the configuration of these features), which suggests a substantial degree of homoplasy. Indeed, previous analyses hypothesized that suspensory species possess more obtuse angles between the vertical canals (Gonzales et al., 2019), as this configuration provides an increased sensitivity for pitch (at the expense of roll) head movements (Muller and Verhagen, 2002a,b,c). The similarities between NHMW 1970/1397/0003, hylobatids, and some atelids (Spoor and Zonneveld, 1998; Gonzales et al., 2019) would thus agree with previous inferences about the locomotor repertoire of this taxon including some degree of suspensory behaviors (Zapfe, 1958; Fleagle, 1983; Langdon, 1986; Rose, 1994; Arias Martorell et al., 2015). In contrast, the more plesiomorphic condition of NBM OE 303III (characterized by tangent lateral and posterior canals, and vertical canals approximating a right angle), also found in *Aegyptopithecus* and some nonsuspensory platyrrhine species, suggests caution when using SC orientation alone for inferring positional behaviors (Perier et al., 2016; contra Malinzak et al., 2012; Berlin et al., 2013).

4.2. *Epipliopithecus* as a stem catarrhine

Epipliopithecus resembles both stem platyrrhines and the stem catarrhine *Aegyptopithecus* in lacking all of the aforementioned hominoid synapomorphies, thereby retaining the plesiomorphic anthropoid condition—a relatively small vestibule, slender SCs, anterosuperiorly nonprojecting anterior portion of the anterior canal, superiorly elongated posterior canal, ampullary portion of the lateral canal not markedly bent superiorly, and long CC. The fact that *Epipliopithecus* lacks hominoid synapomorphies displayed by *Oreopithecus* could still be consistent with a more basal stem hominoid status. However, such an interpretation is contradicted by the retention in *Epipliopithecus* of a superiorly elongated posterior canal and a long CC—contrasting with the rounded posterior canal

and moderately short CC that are synapomorphic of crown catarrhines. The catarrhine status of *Epipliopithecus* and other pliopithecoids is well established based on multiple features, such as the loss of the second premolars and the presence of a C¹/P₃ honing complex (e.g., Harrison, 2013). The catarrhine status of *Epipliopithecus* is further supported by the possession of a rounded anterior canal, which is intermediate between the primitive morphology (superiorly elongated anterior canal) retained by platyrrhines and *Aegyptopithecus*, and the more derived (vertically compressed) morphology synapomorphic of hominoids. In this regard, *Epipliopithecus* is more derived toward crown catarrhines than the propliopithecoid *Aegyptopithecus*, in agreement with other cranial features such as the possession of a partially enclosed tubular ectotympanic in *Epipliopithecus* (e.g., Harrison, 2013).

In summary, based on the morphology of the SCs and vestibule, *Epipliopithecus* is most parsimoniously interpreted as a stem catarrhine more derived than *Aegyptopithecus*, due to its possession of a crown catarrhine synapomorphy—rounded anterior canal—coupled with the lack of two additional crown catarrhine synapomorphies (superiorly elongated posterior canal and long CC) and multiple hominoid and/or hominid synapomorphies as described above. The shapes of the anterior and posterior canals and CC should be considered with caution in light of the intraspecific variability displayed by these characters in some taxa (SOM Table S4). Previous analyses noted a structural relationship between the morphology of these canals and the extension of the subarcuate fossa (Jeffery and Spoor, 2006; Jeffery et al., 2008), and this relationship has been uncritically assumed in some studies (Spoor et al., 2007; Silcox et al., 2009; Gonzales et al., 2019). However, in most cases the fossa simply expands within the space left available from the ossification of the canals, with little or no influence on their shape (Jeffery et al., 2008; see also Urciuoli et al., 2020). In support of the latter hypothesis, we observe meager dissimilarities in the anterior canal morphology of NHMW 1970/1397/0003 and

NBM OE 303III—except for the angle, as discussed above—irrespective of the marked differences in the morphology of the fossa between the two individuals (Zapfe, 1960). While a large amount of morphological variation has been documented within ruminant genera (Mennecart and Costeur, 2016), variation in CC length and shape has not been exhaustively analyzed in primates (Spoor and Zonneveld, 1998; Ekdale 2013; Lee et al., 2013). In the present study, we found considerable intraspecific variation in CC length for some species of monkeys and apes. Nevertheless, our results support a clear morphocline from the ancestral condition (long CC) retained by platyrrhines, *Aegyptopithecus*, and *Epipliopithecus*, to the most derived condition (short CC) characteristic of hominoids, with cercopithecoids displaying an intermediate condition that is likely synapomorphic for crown catarrhines as a whole. Therefore, *Epipliopithecus* SC morphology supports its interpretation as more derived than *Aegyptopithecus* toward crown catarrhines, but excludes a crown catarrhine status and, in particular, a closer relationship with hominoids (unlike in the case of *Oreopithecus*).

5. Conclusions

Our results are in broad agreement with previous analyses suggesting that *Epipliopithecus* displays a ‘typical monkey’ inner ear morphology (Morimoto et al., 2020), while *Oreopithecus* possesses SC and vestibule features derived toward the crown hominoid condition (Urciuoli et al., 2020). At the same time, our study further refines previous comparisons of SC and vestibule morphology between *Epipliopithecus* and other anthropoids, enabling us to test competing hypotheses about the phylogenetic position of this taxon (i.e., stem catarrhine vs. stem hominoid).

From a phenetic viewpoint, for this anatomical area *Epipliopithecus* more closely resembles platyrrhines and the stem catarrhine *Aegyptopithecus*, as well as the reconstructed ancestral catarrhine morphotype. The fact that *Epipliopithecus* shows

greater similarities with the platyrrhine and anthropoid ancestral morphotypes, rather than with those of cercopithecoids or hominoids, supports the view that *Epipliopithecus* is a stem catarrhine instead of a stem hominoid. From a cladistic perspective, this interpretation is confirmed based on a series of crown catarrhine and crown hominoid synapomorphies. *Epipliopithecus* is more parsimoniously interpreted as a stem catarrhine than as a stem hominoid based on the vestibular morphology analyzed here because it lacks several catarrhine and all hominoid synapomorphies. Specifically, the possession of a rounded posterior canal reinforces the view that *Epipliopithecus* is more derived than *Aegyptopithecus* among stem catarrhines.

The information provided by the SCs and vestibule is thus congruent with the ectotympanic morphology of *Epipliopithecus* (see review in Fricano, 2018), which is more plesiomorphic than in crown catarrhines but more derived than in propliopithecoids. Some similarities between *Epipliopithecus* and hylobatids are based on characters that are too variable within species to be of use for phylogenetic assessment. Such features might have evolved independently between some atelids and hylobatids, due to similar locomotor-related selection pressures, and do not support the close phylogenetic link classically hypothesized between pliopithecoids and hylobatids (Hürzeler, 1954; Zapfe, 1960, 1961; Simons and Fleagle, 1973), particularly given that *Epipliopithecus* displays no crown hominoid synapomorphies. We therefore conclude that the SC and vestibular morphology reinforces the most commonly held view that, in accordance with most (Zalmout et al., 2010; Stevens et al., 2013; Nengo et al., 2017) but not all (Alba et al., 2015) recent cladistic analyses, *Epipliopithecus* is best interpreted as a stem catarrhine rather than a stem hominoid.

Acknowledgements

This research has been funded by the Agencia Estatal de Investigación (CGL2016-76431-P and CGL2017-82654-P, AEI/FEDER EU; and BES-2015-071318 to A.U.), the

Generalitat de Catalunya (CERCA Programme, and consolidated research groups 2017 SGR 86 and 2017 SGR 116 GRC), the French Centre National de la Recherche Scientifique, the Leakey Foundation (research grant), and the Synthesys Project (AT-TAF-4689; <http://synthesys3.myspecies.info/>), which is financed by the European Community Research Infrastructure Action under the FP7. Part of the analyses were performed using High Performance Computing resources from BSC (BCV-2020-1-0008). We are grateful to Jose Torres for the technical help provided in the setup of the analysis. We thank the following people for providing or permitting access to CT scans: Ursula Göhlich (*Epipliopithecus* NHMW 1970/1397/0003), Martin Dockner, Loïc Costeur (*Epipliopithecus* NMBOE 303), Lorenzo Rook (*Oreopithecus*), José Braga (human specimens), Lynn Copes, Lynn Lucas, and the MCZ (part of the scans used in the study, funded by NSF DDIG #0925793 and Wenner-Gren Foundation Dissertation Grant #8102 to Lynn Copes), Richard Kay (*Homunculus* and *Dolichocebus*), Timothy Ryan (*Aegyptopithecus*; funded by NSF BCS-0416164 to Timothy Ryan and the Leakey Foundation), and the Division of Fossil Primates of the Duke Lemur Center (*Parapithecus*). We also thank Erik Seiffert and Steven Heritage for providing a digital rendering of *Parapithecus*. Finally, we thank the Editor (Andrea Taylor), the Associate Editor, and three anonymous reviewers for useful comments that helped us to improve a previous version of this paper.

References

- Adams, D.C., 2014. A generalized K statistic for estimating phylogenetic signal from shape and other high-dimensional multivariate data. *Syst. Biol.* 63, 685–697.
- Adams D.C, Collyer, M.L., Kaliontzopoulou, A., 2019. Geomorph: Software for geometric morphometric analyses. R Package Version.
<https://cran.rproject.org/package=geomorph>.

- Alba, D.M., Berning, B., 2013. On the holotype and original description of the pliopithecid *Plesiopliopithecus lockeri* (Zapfe, 1960). *J. Hum. Evol.* 65, 338–340.
- Alba, D.M., Moyà-Solà, S., 2012. A new pliopithecid genus (Primates: Pliopithecoidea) from Castell de Barberà (Vallès-Penedès Basin, Catalonia, Spain). *Am. J. Phys. Anthropol.* 147, 88–112.
- Alba, D.M., Moyà-Solà, S., Malgosa, A., Casanovas-Vilar, I., Robles, J.M., Almécija, S., Galindo, J., Rotgers, C., Bertó Mengual, J.V., 2010. A new species of *Pliopithecus* Gervais, 1849 (Primates: Pliopithecidae) from the Middle Miocene (MN8) of Abocador de Can Mata (els Hostalets de Pierola, Catalonia, Spain). *Am. J. Phys. Anthropol.* 141, 52–75.
- Alba, D.M., Almécija, S., DeMiguel, D., Fortuny, J., Pérez de los Ríos, M., Pina, M., Robles, J. M., Moyà-Solà, S., 2015. Miocene small-bodied ape from Eurasia sheds light on hominoid evolution. *Science* 350, aab2625.
- Almécija, S., Tallman, L., Sallam, H.M., Fleagle, J.G., Hammond, A.S., Seiffert, E.R., 2019. Early anthropoid femora reveal divergent adaptive trajectories in catarrhine hind-limb evolution. *Nat. Commun.* 10, 4778.
- Andrews, P.J., Harrison, T., Delson, E., Bernor, R.L., Martin, L., 1996. Distribution and biochronology of European and Southwest Asian Miocene catarrhines. In: Bernor, R.L., Fahlbusch, V., Mittmann, H. (Eds.), *The Evolution of Western Eurasian Neogene Mammalian Faunas*. Columbia University Press, New York, pp. 168–207.
- Ankel, F., 1965. Der Canalis Sacralis als Indikator für die Länge der Caudalregion der Primaten. *Folia Primatol.* 3, 263–276.
- Arias-Martorell, J., Alba, D.M., Potau, J. M., Bello-Hellegouarch, G., Pérez-Pérez, A., 2015. Morphological affinities of the proximal humerus of *Epipliopithecus vindobonensis* and *Pliopithecus antiquus*: Suspensory inferences based on a 3D geometric morphometrics approach. *J. Hum. Evol.* 80, 83–95.

- Arnold, C., Matthews, L.J., Nunn, C.L., 2010. The 10kTrees website: A new online resource for primate phylogeny. *Evol. Anthropol.* 19, 114–118.
- Beaudet, A., Dumoncel, J., Thackeray, J.F., Bruxelles, L., Duployer, B., Tenailleau, C., Bam, L., Hoffman, J., de Beer, F., Braga, J., 2016. Upper third molar internal structural organization and semicircular canal morphology in Plio-Pleistocene South African cercopithecoids. *J. Hum. Evol.* 95, 104–120.
- Begun, D.R., 2002 The Pliopithecoidea. In: Hartwig, W.C. (Ed.), 2002. *The Primate Fossil Record*. Cambridge University Press, Cambridge, pp. 221–240.
- Begun, D.R., 2017. Evolution of the Pliopithecoidea. In A. Fuentes (Ed.), *The International Encyclopedia of Primatology* (pp. [1-4]): John Wiley & Sons.
- Berlin, J.C., Kirk, E.C., Rowe, T.B., 2013. Functional implications of ubiquitous semicircular canal non-orthogonality in mammals. *PLoS One* 8, e79585.
- Billet, G., Hautier, L., Lebrun, R., 2015. Morphological diversity of the bony labyrinth (inner ear) in extant xenarthrans and its relation to phylogeny. *J. Mammal.* 96, 658–672.
- Blomberg, S.P., Garland, T., Ives, A.R., 2003. Testing for phylogenetic signal in comparative data: behavioral traits are more labile. *Evolution* 57, 717–745.
- Bône, A., Louis, M., Martin, B., Durrleman, S., 2018. Deformetrica 4: an open-source software for statistical shape analysis. In: Reuter, M., Wachinger, C., Lombaert, H., Paniagua, B., Lüthi, M., Egger, B. (Eds.), *Shape in Medical Imaging. Shape MI 2018*. Springer, Cham, pp. 3–13.
- Bookstein, F.L., 2019. Pathologies of between-groups principal components analysis in geometric morphometrics. *Evol. Biol.* 46, 271–302.
- Braga, J., Samir, C., Risser, L., Dumoncel, J., Descouens, D., Thackeray, J.F., Barlesque, P., Oettlé, A., Loubes, J.-M., Fradi, A., 2019a. Cochlear shape reveals that the human organ of hearing is sex-typed from birth. *Sci. Rep.* 9, 10889.

- Bush, E.C., Simons, E.L., Dubowitz, D.J., Allman, J.M., 2004. Endocranial volume and optic foramen size in *Parapithecus grangeri*. In: Ross, C.F., Kay, R.F. (Eds), *Anthropoid Origins: New Visions*. Kluwer/Plenum, New York, pp. 603–614.
- Cardini, A., O’Higgins, P., Rohlf, F.J., 2019. Seeing distinct groups where there are none: Spurious patterns from between-group PCA. *Evol. Biol.* 46, 303–316.
- Cardini, A., Polly, P.D., 2020. Cross-validated between-group PCA scatterplots: A solution to spurious group separation? *Evol. Biol.* 47, 85–95.
- Casanovas-Vilar, I., Alba, D.M., Garcés, M., Robles, J.M., Moyà-Solà, S., 2011. Updated chronology for the Miocene hominoid radiation in Western Eurasia. *Proc. Natl. Acad. Sci. USA* 108, 5554–5559.
- Ciochon, R.L., Corruccini, R.S., 1977. The phenetic position of *Pliopithecus* and its phylogenetic relationship to the Hominoidea. *Syst. Zool.* 26, 290–299.
- Coleman, M.N., Colbert, M.W. 2010. Correlations between auditory structures and hearing sensitivity in non-human primates. *J. Morphol.* 271, 511–532.
- Costeur, L., Grohé, C., Aguirre-Fernández, G., Ekdale, E., Schulz, G., Müller, B., Menecart, B., 2018. The bony labyrinth of toothed whales reflects both phylogeny and habitat preferences. *Sci. Rep.* 8, 7841.
- David, R., Droulez, J., Allain, R., Berthoz, A., Janvier, P., Bennequin, D., 2010. Motion from the past. A new method to infer vestibular capacities of extinct species. *C.R. Palevol* 9, 397–410.
- David, R., Stoessel, A., Berthoz, A., Spoor, F., Bennequin, D., 2016. Assessing morphology and function of the semicircular duct system: introducing new in-situ visualization and software toolbox. *Sci. Rep.* 6, 32772.
- del Rio, J., Aristide, L., dos Reis, S.F., dos Santos, T.M.P., Lopes, R.T., Perez, S.I., 2020. Allometry, function and shape diversification in the inner ear of platyrrhine primates. *J. Mammal. Evol.* <https://doi.org/10.1007/s10914-019-09490-9>.

- Delson, E., Andrews, P.J., 1975. Evolution and interrelationships of the catarrhine primates. In: Lockett, W.P., Szalay, F.S. (Eds.), *Phylogeny of the Primates: A Multidisciplinary Approach*. Plenum Press, New York, pp. 405–446.
- Dumoncel, J., Durrleman, S., Braga, J., Jessel, J.P., Subsol, G., 2014. Landmark-free 3D method for comparison of fossil hominins and hominids based on endocranium and EDJ shapes. *Am. J. Phys. Anthropol.* 153 (S58), 110.
- Durrleman, S., Pennec, X., Trouvé, A., Ayache, N., Braga, J., 2012. Comparison of the endocranial ontogenies between chimpanzees and bonobos via temporal regression and spatiotemporal registration. *J. Hum. Evol.* 62, 74–88.
- Durrleman, S., Prastawa, M., Korenberg, J.R., Joshi, S., Trouvé, A., Gerig, G., 2012. Topology preserving atlas construction from shape data without correspondence using sparse parameters. In: Ayache, N., Delingette, H., Golland, P., Mori, K. (Eds.), *Medical Image Computing and Computer-Assisted Intervention – MICCAI 2012*. Springer, Berlin, pp. 223–230.
- Ekdale, E.G., 2013. Comparative anatomy of the bony labyrinth (inner ear) of placental mammals. *PLoS One* 8, e66624.
- Farris, J.S., 1989. The retention index and the rescaled consistency index. *Cladistics* 5, 417–419.
- Fleagle, J.G., 1983. Locomotor adaptations of Oligocene and Miocene hominoids and their phyletic implications. In: Ciochon, R.L., Corruccini, R.S. (Eds.), *New Interpretations of Ape and Human Ancestry*. Plenum Press, New York, pp. 301–324.
- Fleagle, J.G., 1984. Are there any fossil gibbons? In: Preuschoft, H., Chivers, D.J., Brockelman, W.Y., Creel, N. (Eds.), *The Lesser Apes: Evolutionary and Behavioral Biology*. Edinburgh University Press, Edinburgh, pp. 431–447.
- Fricano, E.E.I., 2018. The primate ectotympanic tube: correlates of structure, function, and development. Ph.D. Dissertation, Johns Hopkins University.

- Fulwood, E.L., Boyer, D.M., Kay, R.F., 2016. Stem members of Platyrrhini are distinct from catarrhines in at least one derived cranial feature. *J. Hum. Evol.* 100, 16–24.
- Gilbert, C.C., Ortiz, A., Pugh, K.D., Campisano, C.J., Patel, B.A., Singh, N.P., Fleage, J.G., Patnaik, R., 2020. New middle Miocene ape (Primates: Hylobatidae) from Ramnagar, India fills major gaps in the hominoid fossil record. *Proc. R. Soc. B* 287, 20201655.
- Glaunès, J.A., Joshi, S., 2006. Template estimation from unlabeled point set data and surfaces for Computational Anatomy. in: Pennec, X., Joshi, S. (Eds.), *MICCAI 2006 Workshop Proceedings. MFCA'06 Workshop. Mathematical Foundations of Computational Anatomy: Geometrical and Statistical Methods for Modelling Biological Shape Variability*. INRIA/MICCAI, Conpenhagen, pp. 29–39.
- Gonzales, L.A., Malinzak, M.D., Kay, R.F., 2019. Intraspecific variation in semicircular canal morphology—A missing element in adaptive scenarios? *Am. J. Phys. Anthropol.* 168, 10–24.
- Grohé, C., Tseng, Z. J., Lebrun, R., Boistel, R., Flynn, J.J., 2015. Bony labyrinth shape variation in extant Carnivora: a case study of Musteloidea. *J. Anat.* 228, 366–383.
- Grohé, C., Lee, B., Flynn, J.J., 2018. Recent inner ear specialization for high-speed hunting in cheetahs. *Sci. Rep.* 8, 1–8.
- Harrison, T., 1982. Small-bodied apes from the Miocene of East Africa. Ph.D. Dissertation, University College London.
- Harrison, T., 1987. The phylogenetic relationships of the early catarrhine primates: a review of the current evidence. *J. Hum. Evol.* 16, 41–80.
- Harrison, T., 2005. The zoogeographic and phylogenetic relationships of early catarrhine primates in Asia. *Anthropol. Sci.* 113, 43–51.

- Harrison, T., 2010. Dendropithecoidea, Proconsuloidea, and Hominoidea (Catarrhini, Primates). In: Werdelin, L. (Ed.), *Cenozoic Mammals of Africa*. University of California Press, Berkeley, pp. 429–469.
- Harrison, T., 2013. Catarrhine origins. In: Begun, D.R. (Ed.), *A Companion to Paleoanthropology*. Blackwell Publishing, Oxford, pp. 376–396.
- Harrison, T., Gu, Y., 1999. Taxonomy and phylogenetic relationships of early Miocene catarrhines from Sihong, China. *J. Hum. Evol.* 37, 225–277.
- Harrison, T., Zhang, Y., Wei, G., Sun, C., Wang, Y., Liu, J., Tong, H., Huang, B., Xu, F., 2020. A new genus of pliopithecoid from the late Early Miocene of China and its implications for understanding the paleozoogeography of the Pliopithecoidea. *J. Hum. Evol.* 145, 102838.
- Harzhauser, M., Kroh, A., Mandic, O., Piller, W. E., Göhlich, U., Reuter, M., Berning, B., 2007. Biogeographic responses to geodynamics: A key study all around the Oligo–Miocene Tethyan Seaway. *Zool. Anz.* 246, 241–256.
- Hürzeler, J., 1954. Contribution a l'odontologie et a la phylogénèse du genre *Pliopithecus* Gervais. *Ann. Paleontol.* 40, 5–63.
- Jeffery, N., Spoor, F., 2006. The primate subarcuate fossa and its relationship to the semicircular canals part I: prenatal growth. *J. Hum. Evol.* 51, 537–549.
- Jeffery, N., Ryan, T.M., Spoor, F., 2008. The primate subarcuate fossa and its relationship to the semicircular canals part II: Adult interspecific variation. *J. Hum. Evol.* 55, 326–339.
- Kay, R.F., Simons, E., Ross, J.L., 2009a. The basicranial anatomy of African Eocene/Oligocene anthropoids. Are there any clues for platyrrhine origins? In: Fleagle, J.G., Gilbert, C.C. (Eds.), *Elwyn Simons: A Search for Origins*. Springer, New York, pp. 125–158.

- Kay, R.F., Fleagle, J.G., Mitchell, T.R.T., Colbert, M., Bown, T., Powers, D.W., 2009b. The anatomy of *Dolichocebus gaimanensis*, a stem platyrrhine monkey from Argentina. *J. Hum. Evol.* 54, 323–382.
- Kay, R.F., 2015. Biogeography in deep time – What do phylogenetics, geology, and paleoclimate tell us about early platyrrhine evolution? *Mol. Phylogenet. Evol.* 82, 358–374.
- Kirk, E.C., Gosselin-Ildari, A.D., 2009. Cochlear labyrinth volume and hearing abilities in primates. *Anat. Rec.* 292, 765–776.
- Kunimatsu, Y., Nakatsukasa, M., Shimizu, D., Nakano, Y., Ishida, H., 2019. Loss of the subarcuate fossa and the phylogeny of *Nacholapithecus*. *J. Hum. Evol.* 131, 22–27.
- Langdon, J.H., 1986. Functional morphology of the Miocene hominoid foot. *Contrib. Primatol.* 22, 239e257.
- Lebrun, R., P. de León, M., Tafforeau, P., Zollikofer, C., 2010. Deep evolutionary roots of strepsirrhine primate labyrinthine morphology. *J. Anat* 216, 368–380.
- Lebrun, R., Godinot, M., Couette, S., Tafforeau, P., Zollikofer, C., 2012. The labyrinthine morphology of *Pronycticebus gaudryi* (Primates, Adapiformes). *Palaeobiodiv. Palaeoenvir.* 92, 527–537.
- Lee, J.Y., Shin, K.J., Kim, J.N., Yoo, J.Y., Song, W.C., Koh, K.S., 2013. A morphometric study of the semicircular canals using micro-CT images in three-dimensional reconstruction. *Anat. Rec.* 269, 834–839.
- Le Maître A., Schuetz, P., Vignaud, P., Brunet, M., 2017. New data about semicircular canal morphology and locomotion in modern hominoids. *J. Anat.* 231, 95–109.
- Macrini, T.E., Flynn, J.J., Ni, X., Croft, D.A., Wyss, A. R., 2013. Comparative study of notoungulate (Placentalia, Mammalia) bony labyrinths and new phylogenetically informative inner ear characters. *J. Anat.* 223, 442–461.

- Malinzak, M.D., Kay, R.F., Hullar, T.E., 2012. Locomotor head movements and semicircular canal morphology in primates. *Proc. Natl. Acad. Sci. USA* 109, 17914–17919.
- Manoussaki, D., Dimitriadis, E.K., Chadwick, R.S., 2006. Cochlea's graded curvature effect on low frequency waves. *Phys. Rev. Lett.* 96, 088701.
- Mennecart, B., Costeur, L., 2016. Shape variation and ontogeny of the ruminant bony labyrinth, an example in Tragulidae. *J. Anat.* 229, 422–435.
- Mennecart, B., Rössner, G. E., Métais, G., DeMiguel, D., Schulz, G., Müller, B., Costeur, L., 2016. The petrosal bone and bony labyrinth of early to middle Miocene European deer (Mammalia, Cervidae) reveal their phylogeny. *J. Morphol.* 277, 1329–1338.
- Mennecart, B., DeMiguel, D., Bibi, F., Rössner, G.E., Métais, G., Neenan, J.M., Wang, S., Schulz, G., Müller, B., Costeur, L., 2017. Bony labyrinth morphology clarifies the origin and evolution of deer. *Sci. Rep.* 7, 13176.
- Mitteroecker, P., Bookstein, F., 2011. Linear discrimination, ordination, and the visualization of selection gradients in modern morphometrics. *Evol. Biol.* 38, 100–114.
- Moyà-Solà, S., Köhler, M., 2000. Comprendere *Oreopithecus bambolii*, un ominoide fossile enigmatico. *Atti Mus. St. Nat. Maremma* 18, 39–65.
- Moyà-Solà, S., Köhler, M., Alba, D.M., 2001. *Egarapithecus narcisoi*, a new genus of Pliopithecidae (Primates, Catarrhini) from the late Miocene of Spain. *Am. J. Phys. Anthropol.* 114, 312–324.
- Morimoto, N., Kanimatsu, Y., Nakatsukasa, M., Ponce de León, M. S., Zollikofer, C. P., Ishida, H., Sasaki, T., Suwa, G., 2020. Variation of bony labyrinthine morphology in Mio–Plio–Pleistocene and modern anthropoids. *Am. J. Phys. Anthropol.* 173, 276–292.
- Muller, M., Verhagen, J.H.G., 2002a. Optimization of the mechanical performance of a two-duct semicircular duct system—Part 1: dynamics and duct dimensions. *J. Theor. Biol.* 216, 409–424.

- Muller, M., Verhagen, J.H.G., 2002b. Optimization of the mechanical performance of a two-duct semicircular duct system—Part 2: excitation of endolymph movements. *J. Theor. Biol.* 216, 425–442.
- Muller, M., Verhagen, J.H.G., 2002c. Optimization of the mechanical performance of a two-duct semicircular duct system—Part 3: the positioning of the ducts in the head. *J. Theor. Biol.* 216, 443–459.
- Nengo, I., Tafforeau, P., Gilbert, C.C., Fleagle, J.G., Miller, E.R., Feibel, C., Fox, D.L., Feinberg, J., Pugh, K.D., Berruyer, C., Mana, S., Engle, Z., Spoor, F., 2017. New infant cranium from the African Miocene sheds light on ape evolution. *Nature* 548, 169–174.
- Pagel, M., 1999. Inferring the historical patterns of biological evolution. *Nature* 401, 877–884.
- Perier, A., Lebrun, R., Marivaux, L., 2016. Different level of intraspecific variation of the bony labyrinth morphology in slow- versus fast-moving Primates. *J. Mammal. Evol.* 23, 353–368.
- R Core Team, 2019. R: A language and environment for statistical computing. R Foundation for Statistical Computing, Vienna.
- Rae, T.C., Johnson, P.M., Yano, W., Hirasaki, E. 2016. Semicircular canal size and locomotion in colobine monkeys: a cautionary tale. *Folia Primatol.* 87, 213–223.
- Revell, L.J., 2012. Phytools: an R package for phylogenetic comparative biology (and other things). *Methods Ecol. Evol.* 3, 217–223.
- Rook, L., Renne, P., Benvenuti, M., Papini, M., 2000. Geochronology of *Oreopithecus*-bearing succession at Baccinello (Italy) and the extinction pattern of european miocene hominoids. *J. Hum. Evol.* 39, 577–582.
- Rook, L., Bondioli, L., Casali, F., Rossi, M., Köhler, M., Moyá Solá, S., Macchiarelli, R., 2004. The bony labyrinth of *Oreopithecus bambolii*. *J. Hum. Evol.* 46, 347–354.

- Rose, M.D., 1994. Quadrupedalism in some Miocene catarrhines. *J. Hum. Evol.* 26, 387–411.
- Russo, G.A., 2016. Comparative sacral morphology and the reconstructed tail lengths of five extinct primates: *Proconsul heseloni*, *Epipliopithecus vindobonensis*, *Archaeolemur edwardsi*, *Megaladapis grandidieri*, and *Palaeopropithecus kelyus*. *J. Hum. Evol.* 90, 135–162.
- Ryan, T.M., Silcox, M.T., Walker, A., Mao, X., Begun, D.R., Benefit, B.R., Gingerich, P.D., Köhler, M., Kordos, L., McCrossin, M.L., Moyà-Solà, S., Sanders, W.J., Seiffert, E.R., Simons, E., Zalmout, I.S., Spoor, F., 2012. Evolution of locomotion in Anthroidea: the semicircular canal evidence. *P. Roy. Soc. B.* 279, 3467–3475.
- Sankhyan, A. R., Kelley, J., & Harrison, T. 2017. A highly derived pliopithecoid from the Late Miocene of Haritalyangar, India. *Journal of Human Evolution* 105, 1–12.
- Savje, F. 2019. distances: tools for distance metrics. <https://cran.r-project.org/web/packages/distances/index.html>.
- Schlager, S., 2017. Morpho and Rvcg – shape analysis in R: R-packages for geometric morphometrics, shape analysis and surface manipulations. In: Zheng, G., Li, S., Székely, G. (Eds.), *Statistical Shape and Deformation Analysis. Methods, Implementation and Applications*. Academic Press, London, pp. 217–256.
- Seiffert, E.R., 2006. Revised age estimates for the later Paleogene mammal faunas of Egypt and Oman. *Proc. Natl. Acad. Sci. USA* 103, 5000–5005.
- Sidlauskas, B., 2008. Continuous and arrested morphological diversification in sister clades of characiform fishes: a phylomorphospace approach. *Evolution* 62, 3135–3156.
- Silcox, M.T., Bloch, J.I., Boyer, D.M., Godinot, M., Ryan, T.M., Spoor, F., Walker, A., 2009. Semicircular canal system in early primates. *J. Hum. Evol.* 56, 315–327.

- Simons, E.L., Fleagle, J.G., 1973. The history of extinct gibbon-like primates. In: Rumbaugh, D.M. (Ed.), *Gibbon and Siamang Vol. 2. Anatomy, Dentition, Taxonomy, Molecular Evolution and Behavior*. Karger, Basel, pp. 121–148.
- Simons, E.L., Seiffert, E.R., Ryan, T.M., Attia, Y., 2007. A remarkable female cranium of the early Oligocene anthropoid *Aegyptopithecus zeuxis* (Catarrhini, Propliopithecidae). *Proc. Natl. Acad. Sci. USA* 104, 8731–8736.
- Spoor, F., Zonneveld, F., 1998. Comparative review of the human bony labyrinth. *Yearb. Phys. Anthropol.* 41, 211–251.
- Spoor, F., Garland, T., Krovitz, G., Ryan, T.M., Silcox, M.T., Walker, A., 2007. The primate semicircular canal system and locomotion. *Proc. Natl. Acad. Sci. USA* 104, 10808–10812.
- Stevens, N.J., Seiffert, E.R., O'Connor, P.M., Roberts, E.M., Schmitz, M.D., Krause, C., Gorscak, E., Ngasala, S., Hieronymus, T.L., Temu, J., 2013. Palaeontological evidence for an Oligocene divergence between Old World monkeys and apes. *Nature* 497, 611–614.
- Swofford, D., 2003. PAUP*. *Phylogenetic Analysis Using Parsimony (*and Other Methods)*. Version 4. Sinauer Associates, Sunderland.
- Szalay, F.S., 1975. Phylogeny of primate higher taxa: the basicranial evidence. In: Lockett, W.P., Szalay, F.S. (Eds.), *Phylogeny of the Primates: A Multidisciplinary Approach*. Plenum Press, New York, pp. 91–125.
- Szalay, F.S., Delson, E., 1979. *Evolutionary History of the Primates*. Academic Press, New York.
- Tejedor, M.F., Rosenberger, A.L., 2008. A neotype for *Homunculus patagonicus* Ameghino, 1891, and a new interpretation of the taxon. *PaleoAnthropology* 2008, 68–82.

- Urciuoli, A., Zanolli, C., Begun, D.R., Almécija, S., Dumoncel, J., Moyà-Solà, S., Alba, D.M., 2019. A deformation-based geometric morphometric analysis of the vestibular apparatus in the Miocene apes *Hispanopithecus laietanus* and *Rudapithecus hungaricus*. *Am. J. Phys. Anthropol.* 168 (S68), 253.
- Urciuoli, A., Zanolli, C., Beaudet, A., Dumoncel, J., Santos, F., Moyà-Solà, S., Alba, D.M., 2020. The evolution of the vestibular apparatus in apes and humans. *eLife* 9, e51261.
- van der Meulen, A.J., García-Paredes, I., Álvarez-Sierra, M.Á., van den Hoek Ostende, L.W., Hordijk, K., Oliver, A., López-Guerrero, P., Hernández-Ballarín, V., Peláez-Campomanes, P., 2011. Biostratigraphy or biochronology? Lessons from the Early and Middle Miocene small Mammal Events in Europe. *Geobios* 44, 309–321.
- Zalmout, I.S., Sanders, W.J., MacLatchy, L., Gunnell, G., Al-Mufarreh, Y.A., Ali, M.A., Nasser, A.-A. H., Al-Masary, A.M., Al-Sobhi, S.A., Nadhra, A.O., Matari, A.H., Wilson, J. A., Gingerich, P. D., 2010. New Oligocene primate from Saudi Arabia and the divergence of apes and Old World monkeys. *Nature* 466, 360–365.
- Zapfe, H., 1958. The skeleton of *Pliopithecus (Epipliopithecus) vindobonensis* Zapfe and Hürzeler. *Am. J. Phys. Anthropol.* 16, 441–457.
- Zapfe, H., 1961. Die Primatenfunde aus der miozänen Spaltenfüllung von Neudorf an der March (Děvínská Nová Ves), Tschechoslowakei. *Schweizer. palaeontol. Abh.* 78, 1–293.
- Zapfe, H., Hürzeler, J., 1957. Die Fauna der miozänen Spaltenfüllung von Neudorf an der March (ČSR.). *Primates. Sitzungsber. Öst. Akad. Wiss. Math. Naturwiss. Kl.* 166, 113–123.